JNC TN8400 2001-018

A Study on Diffusion and Migration of Lead in Compacted Bentonite

—The Effects of Dry Density,Silica Sand Content and Temperature on Diffusion and Migration of Pb-210 in Sodium Bentonite—

March, 2001

TOKAI WORKS
JAPAN NUCLEAR CYCLE DEVELOPMENT INSTITUTE

Ⓐ

JNC TN8400 2001-018
March, 2 0 0 1

A Study on Diffusion and Migration of Lead in Compacted Bentonite —The Effects of Dry Density, Silica Sand Content and Temperature on Diffusion and Migration of Pb-210 in Sodium Bentonite—

Haruo SATO*, Shinya MIYAMOTO*

Abstract

We have studied performance as a diffusion barrier of bentonite which is one of the candidate buffer materials for geological disposal of high-level radioactive waste. Various functions are expected for bentonite and a retardation function in diffusion process of radionuclides released from vitrified waste is also one of them. In this study, diffusion and migration of Pb in bentonite, particularly for the effects of bentonite dry density, silica sand content and temperature on apparent diffusion coefficients (Da) were experimentally studied from the viewpoints of (1) database development and expansion for important nuclides in dose evaluation, (2) confirmation of the validity or conservativity of distribution coefficient (Kd) used in the second progress report, and (3) understanding the mechanism of diffusion and migration behaviour in bentonite.

In diffusion experiments, a Na-bentonite, Kunigel-V1® (Na-smectite, 46-49wt%) was used and the experiments were carried out at dry densities of 0.8, 1.4, 1.6 and 1.8Mg/m^3 and temperatures of 22.5±2.5 and 60±0.1°C by in-diffusion method. The experiments in the systems with silica sand of 30 and 50wt% were also carried out only at a bentonite dry density of 1.6Mg/m^3. Since Pb is much contained in the bentonite, ^{210}Pb which is radioactive, was used as a tracer in all experiments and analysed by a liquid scintillation counter. All experiments were performed in a N_2 atmospheric glove-box (O_2 concentration < 1ppm). Additionally, the background of ^{210}Pb in the bentonite was measured to obtain reliable data. The measurements were carried out as a function of bentonite dry density (0.8, 1.6, 1.8Mg/m^3), saturation period (40-71d) and bentonite slice thickness (0.2-2mm). Furthermore, a HNO_3 solution used for removal of ^{210}Pb from bentonite slices, liquid scintillator and an empty polyethylene vial were also analyzed.

Consequently, no significant difference in counts per minute (cpm) between bentonite dry density, saturation period and slice thickness was found in the background measurements and it was approximately constant between 2 and 4cpm over the experimental conditions. The cpm values for HNO_3, liquid scintillator and an empty polyethylene vial were also approximately the same degree as those for bentonite. This indicates that obtained cpm is neither originated from bentonite nor HNO_3. The diffusion of ^{210}Pb is quite slow and the distance penetrated in the diffusing period (~210d) was several mm at the maximum. The obtained Da values, in a range of 10^{-17} to 10^{-15}m^2/s order at 22.5°C, decreased with increasing bentonite dry density and showed a tendency to increase with increasing silica sand content in bentonite and temperature. Furthermore, Da values were well correlative with smectite partial density which was defined by the density of only smectite part in bentonite. This indicates that Pb diffusion is predominantly controlled by the properties in part of smectite. The conservativity of Kd for Pb used for the reference case in the second progress report was confirmed from comparison between Kd calculated from obtained Da and that used in the second progress report.

* Radiochemistry Group/Barrier Performance Group, Waste Isolation Research Division, Waste Management and Fuel Cycle Research Center, Tokai Works, Japan Nuclear Cycle Development Institute

JNC TN8400 2001-018
2 0 0 1 年 3 月

圧縮ベントナイト中の鉛の拡散移行に関する研究
—Na 型ベントナイト中の鉛(Pb-210)の拡散移行に及ぼす乾燥密度、珪砂混合率、温度の影響—
(研究報告)

佐藤治夫*、宮本真哉*

要　旨

高レベル放射性廃棄物の地層処分における緩衝材の候補材の１つであるベントナイトの拡散バリアとしての性能について研究した。ベントナイトには様々な機能が期待されており、この内、ガラス固化体から溶出した放射性核種の拡散過程における遅延機能もその１つである。本研究では、ベントナイト中での Pb の拡散移行、特に見掛けの拡散係数(Da)に及ぼすベントナイトの乾燥密度、珪砂混合率、温度の影響について、(1)線量評価上、重要核種に対するデータベースの整備拡充、(2)第 2 次取りまとめにおいて設定した分配係数(Kd)の妥当性あるいは保守性の確認、(3)ベントナイト中の拡散移行挙動に関する現象解明、の観点から実験的に検討した。

実験は、Na 型ベントナイト(クニゲル V1®：Na スメクタイト含有率 46～49wt%)を用い、乾燥密度 0.8, 1.4, 1.6, 1.8Mg/m^3、温度 22.5 及び 60°C に対して In-diffusion 法により行った。また、乾燥密度 1.6Mg/m^3 に対しては、30 及び 50wt%の珪砂を混合させた系についても行った。Pb はベントナイト中に多く含まれていることから、測定においては放射性の ^{210}Pb をトレーサとし分析は液体シンチレーションカウンタにより行った。全ての実験は N_2 雰囲気のグローブボックス(酸素濃度＜1ppm)内で行った。さらに、信頼性のあるデータを得るため、ベントナイト中の ^{210}Pb のバックグラウンドを定量した。バックグラウンドの測定は、乾燥密度(0.8, 1.6, 1.8Mg/m^3)、含水期間(40～71d)、ベントナイトのスライス厚(0.2～2mm)をパラメータとした。加えて、ベントナイトのスライス片からの ^{210}Pb の抽出に用いた硝酸、液体シンチレータ、空のポリバイアルについても分析した。

その結果、ベントナイト乾燥密度、含水期間、スライス厚さによる計数率の差は見られず 2～4cpm とほぼ一定であった。硝酸、液体シンチレータ、空のポリバイアルについてもベントナイトと同程度であった。このことは、得られた計数率がベントナイトや硝酸などの試薬に起因しないことを示している。^{210}Pb の拡散は非常に遅く、拡散期間内(～210d)で拡散した距離は、最大でも数 mm 程度であった。得られた Da は、室温に対しては 10^{-17}～10^{-15}m^2/s オーダーであり、ベントナイト乾燥密度の増加に伴って減少し、珪砂混合率の増加及び温度の上昇に伴って増加する傾向を示した。また、Da はベントナイト中のスメクタイト部分のみの密度によって定義されたスメクタイト部分密度とよく相関した。このことは、Pb の拡散がスメクタイト部分の特性に支配されることを示している。さらに、Da から求めた Kd と第2次取りまとめにおけるレファレンスケースに対して設定された Kd との比較から、設定値の保守性が確認された。

＊核燃料サイクル開発機構　東海事業所　環境保全・研究開発センター
処分研究部　放射化学研究グループ

Contents

Figures

Tables

1. INTRODUCTION

The second progress report for a technical feasibility of the geological disposal of high-level radioactive waste (HLW) [1] was submitted to the government on November 26 in 1999 and a review by the government also simultaneously started. And the review by the government also finished in October, 2000. Since various analysis cases for variety of geological environmental condition, groundwater and design condition have been considered for safety analysis of geological disposal system in the second progress report, those input data have been determined based on a lot of data and information accumulated so far. Particularly, since data for radionuclide diffusion and migration in buffer material and rocks which are considered to finally affect also dose evaluation play important role on the safety analysis, thermodynamic database (TDB) [2], sorption database (SDB) [3] and diffusivity database (DDB) [4] which measured data reported to date were summarized, were developed and input datasets have been conservatively determined, considered uncertainty based on those measurement data.

However, it became clear from the database development that measured data for all analysis cases do not exist. Thereon, cases that no measurement datum exists and those that the reliability of data is controversial, are based on chemical analogy and existing knowledge, and some future studies remain from the viewpoint of reliability and data accumulation. For example, Kd values for Pb, Ac, Th, Pa and Cm onto bentonite, of which measured Da values do not exist, have been determined based on chemical analogy and the similarity of species in porewater [1]. For the effect of silica sand mixture to bentonite on diffusion, particularly, on Da, has been taken into account based on measured data reported to date. Also with respect to the effect of temperature on diffusion (effective diffusion coefficient (De) in the second progress report) has been corrected based on an activation energy for average diffusion coefficient in free water (Dw) which is shown by the following differential equation [5].

$$\frac{d\ln \mathrm{D}}{d\mathrm{T}} = \frac{\Delta \mathrm{E_a}}{\mathrm{RT}^2} \qquad (1\text{-}1)$$

Where D is the diffusion coefficient (m^2/s), T is the absolute temperature (K), ΔEa is the activation energy (J/mol), and R is the gas constant (8.314 J/mol/K).

In the second progress report, an activation energy of 15.05 kJ/mol (3.60 kcal/mol) as an average value has been adopted to correct temperature on De, because it is said that the activation energy for all electrically conductive processes in water except the processes that involve H^+ or OH^- is approximately 15.05 kJ/mol [6]. In this case, the temperature correction of De was carried out based on the following equation which is the analytical solution of equation (1-1).

$$\mathrm{D} = \mathrm{D_f} \cdot exp\left(-\frac{\Delta \mathrm{E_a}}{\mathrm{RT}}\right) \qquad (1\text{-}2)$$

Where Df is the frequency factor.

Sorption-diffusion behaviour of Pb in bentonite is one of the elements, of which behaviours are not familiar and is presently unclear. In the second progress report, Kd of Pb onto bentonite has been determined, based on analogue data of Ni which is one of the transition elements and takes the same valence as that of Pb.

With respect to diffusion on Pb in compacted bentonite, although studies on leaching-diffusion coupling experiments of Pb from a container, into which pure Pb was cast and then sealed with a screw lid in bentonite at a bentonite dry density of 1.5 Mg/m^3, have been reported, the width of variation in the obtained Da values is quite large in a range of 10^{-15} to 10^{-11} m^2/s order and the reliability of those data is low [7, 8]. In addition, since much Pb is contained in bentonite and also exists in natural environment, it is difficult to obtain diffusion data by using a stable isotope.

Thereon, in this study, Da values of Pb in compacted bentonite were measured as a function of bentonite dry density, silica sand content in bentonite and temperature using ^{210}Pb as a tracer to confirm the validity or conservativity of Kd on the bentonite and to make progress in addtional data accumulation as a link in the chain of a follow-up of the second progress report.

2. EXPERIMENTAL

2.1 Experimental Conditions

The diffusion experiments were carried out by in-diffusion method [e.g. 9, 10]. **Tables I** and **II** show experimental conditions for the diffusion experiments of Pb in bentonite and experimental matrix for the diffusion experiments, respectively. Although Pb is not sensitive to redox condition, all experiments were carried out in a N_2 glove-box, in which oxygen concentration was kept < 1 ppm to reproduce a disposal condition (an anaerobic condition). A sodium bentonite, Kunigel-V1® (Kunimine Industries Co. Ltd.), which a lot of data regarding fundamental properties and diffusion have been reported and has been used as a reference for the reference case in the second progress report, was used as a bentonite sample in this study. The experiments were carried out at bentonite dry densities of 0.8, 1.4, 1.6 and 1.8 Mg/m^3. In addition, the experiments in the systems with silica sand of 30 and 50 wt% were also carried out at a bentonite dry density of 1.6 Mg/m^3. The degassed distilled water was prepared by bubbling more than 24 hours with atmospheric gas in the glove-box. The tracer solution containing ^{210}Pb (purchased from AEA Technology plc) was neutralized at around pH7 by 1N NaOH before the experiments, because original solvent was 1.2M HNO_3 and possible to damage the surface of bentonite when the tracer solution is pipetted, although described in detail later. All experiments were carried out at room temperature (22.5±2.5 °C) and 60±0.1 °C (oven) to obtain the temperature dependencies of Da values and the effect of temperature on Da values.

Table I Experimental conditions for the diffusion experiments of Pb in bentonite

Bentonite :	Kunigel-V1® (composition of Na-smectite, 46–49wt%)
Dry density :	0.8, 1.4, 1.6, 1.8 Mg/m^3
Composition of silica sand :	30, 50wt% (mixed silica sand with particle sizes of 1–5mm and 0.1–1mm at a mixture ratio of 1:1) (only at a dry density of 1.6 Mg/m^3)
Tracer :	^{210}Pb (β^- decay, half-life: 22.3y (17keV(84%), 63.5keV(16%)): 200kBq/5ml 1.2MHNO_3 solution → neutralization treatment carrier: 20ppm $Pb(NO_3)_2$, $Bi(NO_3)_3$
Introduced tracer quantity :	815 Bq/experiment (0.05ml stock solution, neutralized)
Temperature :	room temperature (22.5±2.5 °C) 60±0.1 °C (oven)
Atmosphere :	anaerobic conditions (N_2 atmosphere) (O_2 concentration < 1 ppm)
Saturated porewater :	degassed distilled water
Experimental period :	14–210 days (n=1: 14–27 days, n=2: 78–210 days)
Producibility :	n=2

Table II Experimental matrix for the diffusion experiments of Pb in bentonite

Bentonite dry density (Mg/m^3)			0.8	1.4	1.6	1.8
Content of silica sand (wt%)	0	room*	○	○	○	○
		60°C	○	○	○	○
	30	room*			○	
		60°C			○	
	50	room*			○	
		60°C			○	

* The temperature was monitored (22.5±2.5°C).
The experiments were carried out in duplicate for each condition.

2.2 Neutralization of Tracer Solution

The tracer solution containing ^{210}Pb was neutralized by 1N NaOH before diffusion experiments to prevent around the surface of bentonite from damaging when the tracer solution, of which solvent is 1.2M HNO_3 was pipetted, as described in **2.1**. Before the neutralization of the tracer solution, a titration test for neutralization was carried out to determine the volume of 1N NaOH to be added. Although the volume of the tracer solution is 5ml, it is difficult to carry out the titration test, because the volume is too little. Therefore, a titration test was carried out with respect to a solution with a volume of 10 times as much. A 1.2M HNO_3 solution of a volume of 50 ml was prepared and a titration test by 1N NaOH was then carried out.

Figure 1 shows the result of the titration test (neutralization curve). Based on the result of this titration test, a volume of 1N NaOH to be added to the actual tracer solution was determined. In this case, buffer index which is the parameter to quantitatively express the pH change when a pH adjustment agent was added to the solution near the neutralization point, is defined as the following equation.

$$\delta = \frac{\Delta N}{\Delta pH} \qquad (2.2\text{-}1)$$

Where δ is the buffer index, expressing the amount of agent to be needed to change unit pH, ΔpH is the pH change when the pH adjustment agent was added by ΔN, and ΔN is the amount of the pH adjustment agent added to the solution (mgeq/l).

When the δ is large, the pH adjustment of the solution is easy, but when the δ is small, the pH adjustment of the solution is generally difficult. The δ was approximately estimated to be 25.5 from neutralization curve in this titaration test. This means that a 1N NaOH solution of 25.5 mg is needed to raise unit pH around neutral pH.

Although a 1N NaOH solution of 65.75 ml was totally added to a 1.2M HNO_3 solution of a volume of 50 ml for neutralization, actual volume of the tracer solution is 1/10 of the HNO_3 solution prepared for the titration test. Therefore, a 1N NaOH solution of 6.575 ml which is equivalent to 1/10 of solution volume used in the titration test

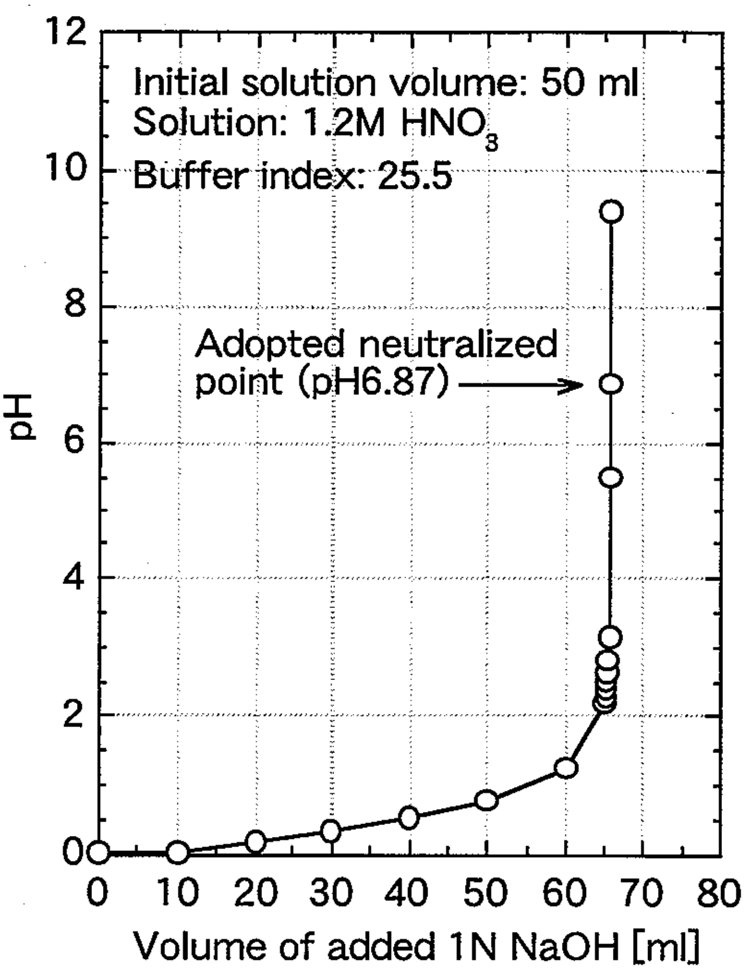

Figure 1 A Correlation between measured pH and solution volume of added 1N NaOH in the titration test (neutralization curve)

was added for actual neutralization. The pH of the solution in the case was 6.87.

2.3 Diffusion Experiments

The diffusion experiments were carried out by in-diffusion method as described in **2.1.** **Figures 2** and **3** show a sectional view of a diffusion column and the diffusion test flow, respectively. The diffusion column is made of acrylic resin and a cylindrical space of 20 mm in diameter and 20 mm in thickness, in which bentonite is filled, is cored inside of the diffusion column. Throughout the saturation of the bentonite, the bentonite contacted with degassed distilled water through alumina ceramic filters (alumina sintered filter) with a pore size of 2 μm used to prevent the bentonite from the swelling, as shown in **Figure 2**.

The bentonite powder was firstly dried at 110 °C more than 24 hours in an oven and filled into the cylindrical space of the diffusion column together with silica sand to obtain contents of 30 and 50 wt% after being mixed enough with an agate mortar. The filling of the bentonite with high density such as samples higher than 1.4 Mg/m^3 was carried out by using a hydraulic press [11]. The diffusion column filled with bentonite and silica sand was removed for air by exchanging with N_2 gas several times in a vacuum chamber and then transferred to the glove-box [12]. The diffusion column with bentonite was then saturated with degassed distilled water for 23 or 24 days under atmospheric pressure after being degassed a half hour in a vacuum chamber.

After the saturation of the bentonite, a small amount of a tracer solution (50μl: 815 Bq), which was neutralized by 1N NaOH in advance based on the result of titration test, was pipetted on the surface of one end of each bentonite and a blind lid was then sealed shut. The other end of the column was also similarly closed up with a blind lid to get air tightness and allowed to diffuse for 14 to 210 days at room temperature (22.5±2.5 °C) and 60±0.1 °C (in an oven).

At the end of the experiment the smaller blind lid was taken off and a pushing tool with gauge was connected. The cylindrical bentonite in the diffusion column was pushed out by the pushing tool and cut with a knife into 0.2 to 4 mm pitched slices. Each slice was immediately weighed to calculate accurately the thickness of the slice and distance sliced from the surface of bentonite where tracer solution was pipetted. The slices were immersed in a 5 ml 1M HNO_3 solution in a polyethylene bottle for 1 to 8 days to extract tracer (Pb) from the slices and then a sample of 1 ml was taken from the supernatant of the suspension. The sampled solution was mixed enough with a liquid scintillator (mixture of alkyl-naphthalenes, ULTIMA GOLD™ XR, PACKARD) of 3 ml in a polyethylene vial (high density polyethylene, Pico Pro Vial-4ml)) (PACKARD 6000252) and the concentration of ^{210}Pb was analyzed with a liquid scintillation counter (PACKARD TRI-CARB 2770TR/SL) for a half hour in an energy range of 0 to 20 keV. The concentration profiles in the bentonite were determined based on the analyzed data.

In this study, the slicing of bentonite was carried out by a pushing tool with counter gauge. However, it is difficult to accurately slice with constant thickness due to pushing error. Therefore, depth sliced from the surface of bentonite was determined based on each slice weight in this study. This explanation to determine the depth from the surface of bentonite will be made later.

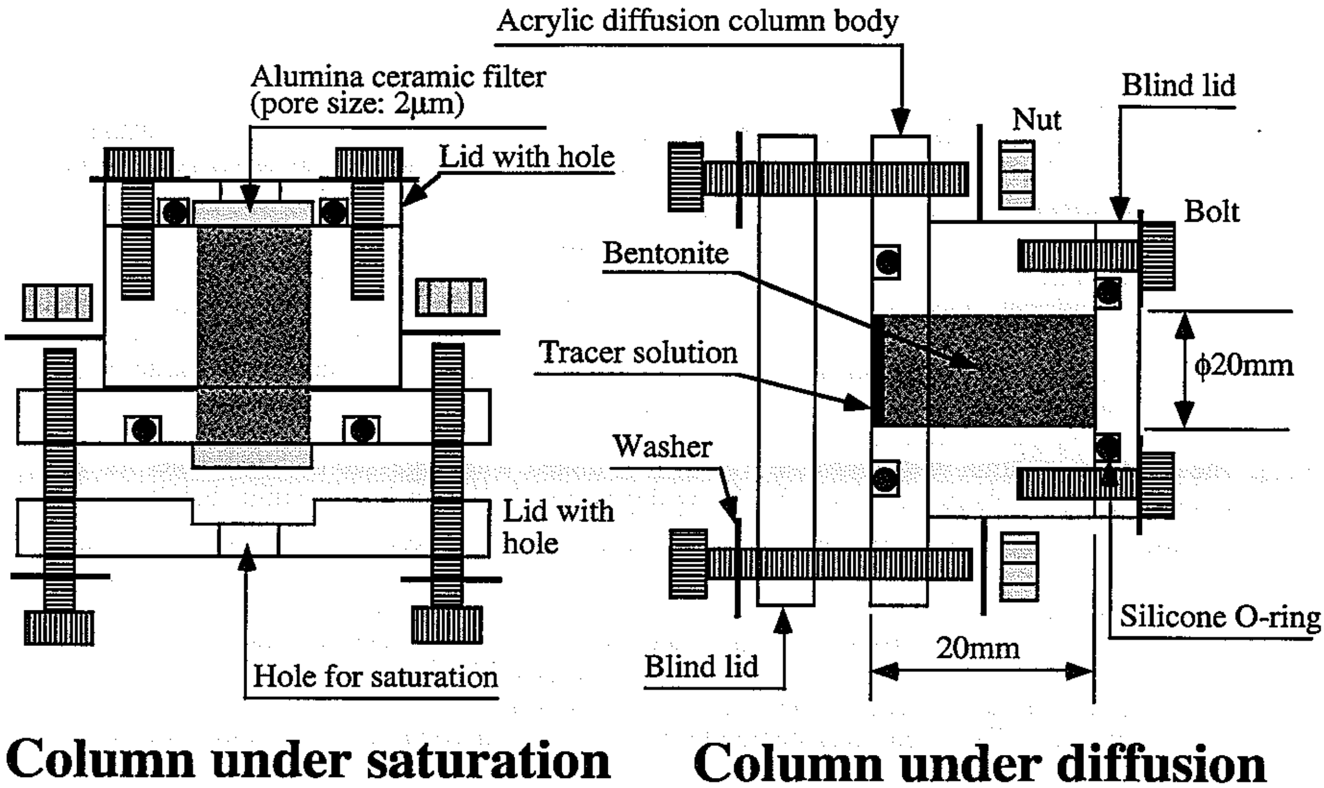

Figure 2 A sectional view of a diffusion column (left column shows an image of diffusion column under saturation and right column shows an image of the diffusion column under diffusion)

The saturation and diffusion experiments were carried out in a N_2 atmospheric glove-box.

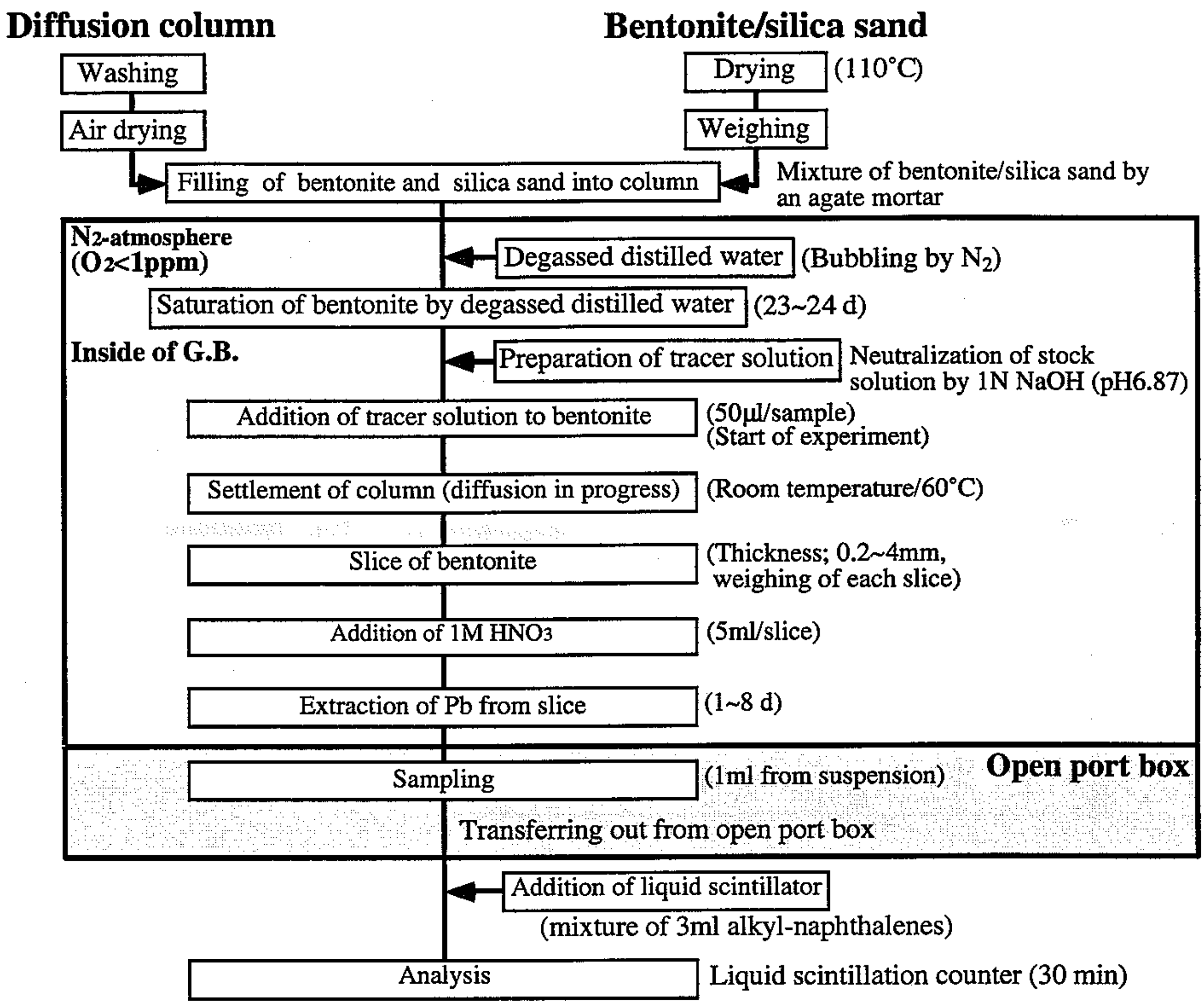

Figure 3 Diffusion test flow for ^{210}Pb in bentonite

Figure 4 shows an image of a model to calculate distance from the surface of bentonite where tracer solution was pipetted. If the length of the bentonite specimen is L and the weight for the i-th slice from the surface of bentonite where tracer solution was pipetted, the thickness for the i-th slice is calculated by the following equation.

$$L_i = \frac{W_i}{\left(\sum_{i=1}^{n} W_i\right)} \cdot L \qquad (2.3\text{-}1)$$

Where Li is the thickness for the i-th bentonite slice (mm), Wi is the weight for the i-th bentonite slice (g), n is the number of total slice (–), and L is the length of the bentonite specimen (mm).

Distance from the surface of bentonite where tracer solution was pipetted for the i-th bentonite slice, Xi, is calculated as follows:

$$X_i = X_{i-1} + \left(\frac{L_{i-1} - L_i}{2}\right). \qquad (2.3\text{-}2)$$

Where Xi is the distance from the surface of bentonite where tracer solution was pipetted for the i-th bentonite slice (mm).

From equations (2.3-1) and (2.3-2), distance from the surface of bentonite where tracer was pipetted, is derived as follows.

$$X_i = X_{i-1} + \frac{W_{i-1} - W_i}{\left(2\sum_{i=1}^{n} W_i\right)} \cdot L \qquad (2.3\text{-}3)$$

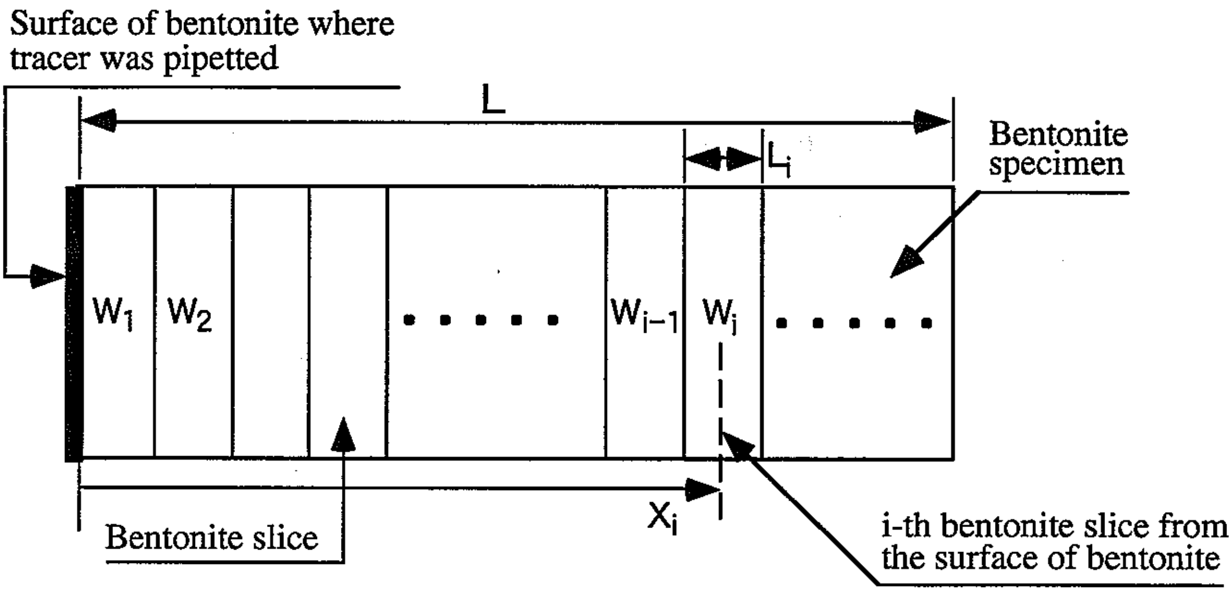

Figure 4 An image of a model to calculate distance from the surface of bentonite where tracer was pipetted

2.4 Background Measurements of ^{210}Pb in Bentonite

The background measurments of ^{210}Pb in bentonite were carried out as a function of bentonite dry density (0.8, 1.6, 1.8 Mg/m^3), saturation (immersion) (40–71 d) period and bentonite slice thickness (0.2–2 mm). **Tables III** and **IV** show experimental conditions for the background measurments of ^{210}Pb in the bentonite and experimental matrix for the background measurments, respectively.

The same type of acrylic diffusion column was used in the background measurements. The drying and filling of bentonite were carried out in the same way as diffusion experiments of ^{210}Pb. The diffusion column with bentonite were immersed with degassed distilled water for 40 to 71 days in a N_2 atmospheric glove-box. At the end of each immersion period, the cylindrical bentonite in the column was sliced into 0.2 to 2 mm and weighed to calculate accurately slice thickness. The immersion of the slices in a 5 ml 1M HNO_3 solution, sampling from the suspension and analysis were carried out in the same as diffusion experiments of ^{210}Pb. Additionally, a HNO_3 solution used for removal of Pb from bentonite slices, a high purity HNO_3 solution with liquid scintillator, liquid scintillator and an empty polyethylene vial were also analyzed to identify the cause of backgroud.

Table III Experimental conditions for the background measurements of ^{210}Pb in bentonite

Bentonite :	Kunigel-V1®
Dry density :	0.8, 1.6, 1.8 Mg/m^3
Temperature :	room temperature
Atmosphere :	anaerobic conditions (N2 atmosphere) (O2 concentration < 1 ppm)
Saturated porewater :	degassed distilled water
Saturation period :	40, 50, 71 days
Slice thikness :	0.2, 0.5, 1.0, 2 mm

Table IV Experimental matrix for the background measurments of ^{210}Pb in bentonite

Bentonite dry density (Mg/m^3)		0.8	1.6	1.8
Saturation period (d)	40	○	○	○
	50	○	○	○
	71	○	○	○

2.5 Standard Sample Preparation of ^{210}Pb

A standard sample loaded ^{210}Pb was prepared to determine the energy range for analysis and detection efficiency. The standard solution was prepared by adding a 3 ml liquid scintillator to a 1 ml 1M HNO_3 solution with a radioactivity of 815 Bq.

3. DIFFUSION THEORY

The calculations of Da values were based on the Fickian law [13]. The diffusion equation for one-dimensional non-steady state considered decay term is generally expressed by the following equation.

$$\frac{\partial C}{\partial t} = \frac{\partial}{\partial x}\left(Da\frac{\partial C}{\partial x}\right) - \lambda \cdot C \qquad (3\text{-}1)$$

Assuming that Da is independent of distance and the half-life is long enough compared with experimental period, equation (3-1) is approximately arranged as the following equation.

$$\frac{\partial C}{\partial t} = Da\frac{\partial^2 C}{\partial x^2} = \left(\frac{De}{\alpha}\right)\frac{\partial^2 C}{\partial x^2} \qquad (3\text{-}2)$$

Where C is the radioactivity concentration of the tracer in the bentonite (cpm/m^3), t is the diffusing time (s), x is the distance from the source (m), Da is the apparent diffusion coefficient (m^2/s), λ is the decay constant (1/s), De is the effective diffusion coefficient (m^2/s), α is the rock capacity factor (= $\varepsilon+\rho d \cdot Kd$)(–), ρd is the bentonite dry density (Mg/m^3), Kd is the distribution coefficient (m^3/Mg), and ε is the porosity (m^3/m^3).

With respect to soluble elements, the analytical solution in case of an instantaneous planar source can be applied for the calculations of Da values. On the other hand, with respect to elements which solubilities in the porewater of bentonite are low, there is a possibility that precipitation occurs on the surface of the bentonite after the tracer solution was pipetted. In this case, the boundary condition is presumed to be controlled by the solubility of the tracer.

With respect to one-dimensional diffusion of a planar source consisting of a limited amount of substance in a cylinder of infinite length, the analytical solution for equation (3-2), based on initial and boundary conditions, is given by the following equation [13].

Initial condition
$C(t, x) = 0,\ t = 0,\ x \neq 0$
Boundary condition
$C(t, x) = 0,\ t > 0,\ |x| = \infty$

$$M = \int_0^\infty C\,dx$$

$$C = \frac{M}{\sqrt{\pi Da \cdot t}} exp\left(-\frac{x^2}{4Da \cdot t}\right) \qquad (3\text{-}3)$$

Where M is the total amount of tracer added per unit aera of the bentonite (cpm/m^2). This analytical equation is applied for diffusion in one direction from one source.

With respect to diffusion in 2 directions from one source, the following analytical equation is applied.

Initial condition
$C(t, x) = 0,\ t = 0,\ x \neq 0$
Boundary condition
$C(t, x) = 0,\ t > 0,\ |x| = \infty$

$$M = \int_{-\infty}^{\infty} C\,dx = \int_{-\infty}^{0} C\,dx + \int_0^\infty C\,dx = 2\int_0^\infty C\,dx$$

$$C = \frac{M}{2\sqrt{\pi Da \cdot t}} exp\left(-\frac{x^2}{4Da \cdot t}\right) \qquad (3\text{-}4)$$

From equation (3-4), taking lnC and x^2 as the vertical and horizontal axes, respectively, the slope can be used to derive Da at the diffusing time.

If bentonite sample is assumed to be a semi-infinite medium, the analytical solution for the boundary condition of a constant concentration is derived as the following equation on the basis of initial and boundary conditions [13].

Initial condition
$C(t, x) = 0,\ t = 0,\ |x| \neq 0$
Boundary condition
$C(t, x) = Co,\ t \geq 0,\ x = 0$
$C(t, x) = 0,\ t > 0,\ |x| = \infty$

$$\frac{C}{Co} = erfc\left(\frac{|x|}{2\sqrt{Da \cdot t}}\right) = 1 - erf\left(\frac{|x|}{2\sqrt{Da \cdot t}}\right) \qquad (3\text{-}5)$$

Where Co is the boundary concentration (cpm/m^3), *erf* is the error function, and *erfc* is the complementary error function.

The error function is here defined by the following equations.

$$erf\left(\frac{|x|}{2\sqrt{Da \cdot t}}\right) = 1 - erfc\left(\frac{|x|}{2\sqrt{Da \cdot t}}\right) = \frac{2}{\sqrt{\pi}} \int_0^{\frac{|x|}{2\sqrt{Da \cdot t}}} exp\left(-z^2\right) dz \qquad (3\text{-}6)$$

And

$$\lim_{|x| \to \infty} \int_0^{\frac{|x|}{2\sqrt{Da \cdot t}}} exp\left(-z^2\right) dz = \frac{\sqrt{\pi}}{2}. \qquad (3\text{-}7)$$

Analytical method to determine Da was discussed from the concentration profiles of ^{210}Pb in bentonite obtained in this series of experiments. Comparing the concentrations near the surface of bentonite where tracer solution was pipetted, no concentration gap with time or temperature for the same bentonite density was found. This indicates that boundary concentration is constant. In addition, the solubility of Pb in the porewater of bentonite was predicted to be 2x10^{-6} M (solubility limiting solid phase: $PbCO_3$) [1, 5]. This solubility was proved also from preliminary tests conducted for the same condition in the past and it is considered to be reliable. The tracer solution used for the experiments includes 20 ppm $Pb(NO_3)_2$ (equivalent to 6.0x10^{-5} M) as a carrier and bentonite also contains much Pb. Therefore, it is considered that Pb precipitates at the surface of bentonite when tracer solution was introduced and boundary concentration is controlled by the solubility of Pb.

The Da values for ^{210}Pb were determined by a least squares fitting to the concentration profiles of ^{210}Pb in bentonite based on equation (3-5) in this study. Since equation (3-5) is the infinite arithmetrical series, it is difficult to determine Da values by directly fitting to equation (3-5). Therefore, Da values for ^{210}Pb were determined by discretizing equation (3-2) in this study.

4. NUMERICAL ANALYSES BASED ON FINITE DIFFERENCE METHOD

In this study, Da values were determined by a least squares fitting based on a finite difference method (FDM) [13]. The details is described as follows. Analytical method by explicit difference method which can be forwardly calculated is here briefly explained among finite difference methods.

4.1 Difference Approximation for Derivative

When a function f(x) and the derivative are both the finite continuous functions, we can express as follows based on the Taylor's principle.

$$f(x+\Delta x)=f(x)+\Delta x\cdot f'(x)+\frac{1}{2}\Delta x^2\cdot f''(x)+\frac{1}{6}\Delta x^3\cdot f'''(x)+\cdots\cdots+\frac{1}{n!}\Delta x^n\cdot f^{(n)}(x)+\cdots \qquad (4.1\text{-}1)$$

And

$$f(x-\Delta x)=f(x)-\Delta x\cdot f'(x)+\frac{1}{2}\Delta x^2\cdot f''(x)-\frac{1}{6}\Delta x^3\cdot f'''(x)+\cdots\cdots+\frac{(-1)^n}{n!}\Delta x^n\cdot f^{(n)}(x)+\cdots. \qquad (4.1\text{-}2)$$

Adding equations (4.1-1) and (4.1-2),

$$f(x+\Delta x)+f(x-\Delta x)=2f(x)+\Delta x^2\cdot f''(x)+O(\Delta x^4) \qquad (4.1\text{-}3)$$

Where $O(\Delta x^4)$ signifies the term including the terms higher than the 4th order for Δx.

If $O(\Delta x^4)$ is small enough to be able to neglect compared with the terms lower than the 4th order for Δx, equation (4.1-3) is re-arranged as follows.

$$f''(x)=\left(\frac{d^2 f(x)}{dx^2}\right)_{X=X}\cong\frac{f(x+\Delta x)-2f(x)+f(x-\Delta x)}{\Delta x^2} \qquad (4.1\text{-}4)$$

The leading error for the light side of equation in this equation depends on the degree of Δx^2. By subtracting equation (4.1-2) from equation (4.1-1) and neglecting the terms higher than the 3rd order for Δx,

$$f'(x)=\left(\frac{d f(x)}{dx}\right)_{X=X}\cong\frac{f(x+\Delta x)-f(x-\Delta x)}{2\Delta x} \qquad (4.1\text{-}5)$$

is derived. The leading error in this equation depends on the degree of Δx.

Figure 5 shows a conceptual model for difference approximation. Equation (4.1-5) approximates the slope of tangent at a point P by the slope of chord AB and is called a central difference approximation. Besides, the slope of tangent at the point P can be expressed also by a forward difference approximation formula approximating by chord PB or a backward difference approximation formula approximating by chord AP as follows.

$$f'(x)\cong\frac{f(x+\Delta x)-f(x)}{\Delta x} \qquad (4.1\text{-}6)$$

$$f'(x)\cong\frac{f(x)-f(x-\Delta x)}{\Delta x} \qquad (4.1\text{-}7)$$

It is clear that the leading error for equations (4.1-6) and (4.1-7) are $O(\Delta x^4)$.

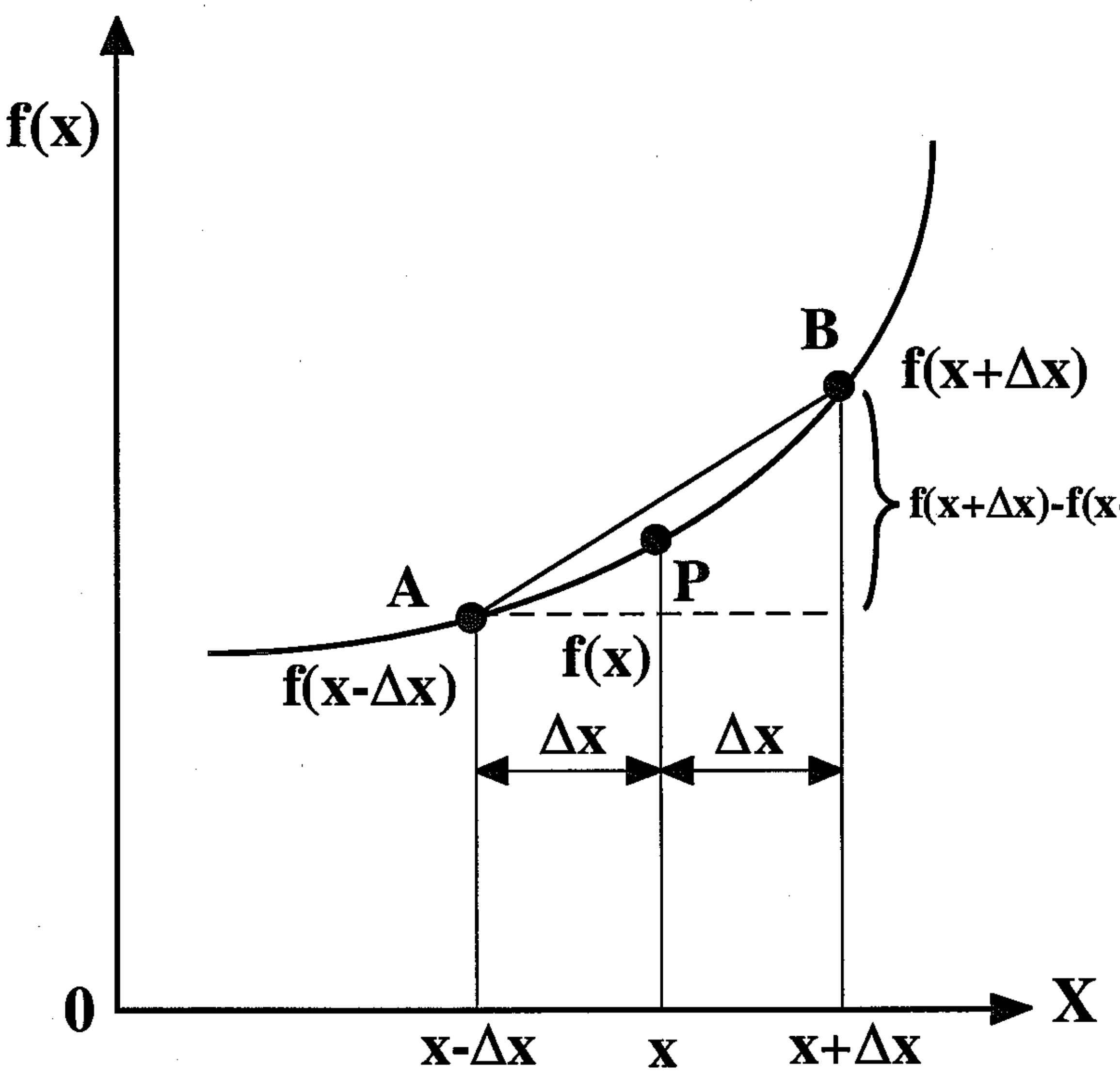

$$f'(x)=\lim_{\Delta x \to 0}\frac{f(x+\Delta x)-f(x-\Delta x)}{2\Delta x}=\lim_{\Delta x \to 0}\frac{f(x+\Delta x)-f(x)}{\Delta x}$$

$$=\lim_{\Delta x \to 0}\frac{f(x)-f(x-\Delta x)}{\Delta x}$$

Figure 5 A conceptual model for difference approximation by f(x)-x graph

4.2 Governing Equations

The Fickian first law for one-dimensional diffusion equation is expressed by the following equation.

$$J = -De\left(\frac{\partial Cp}{\partial x}\right) = -\frac{De}{\alpha}\left(\frac{\partial C}{\partial x}\right) = -Da\left(\frac{\partial C}{\partial x}\right) \qquad (4.1\text{-}8)$$

Where J is the diffusional mass flux (cpm/m²/s), and Cp is the radioactivity concentration of tracer in the porewater of bentonite (cpm/m³).

The concentration profile of tracer in bentonite is calculated by equation (3-2). Initial and boundary conditions in this computation are given as follows.

Initial condition
$C(t, x) = 0,\ t = 0,\ |x| \neq 0$
Boundary condition
$C(t, x) = Co,\ t \geq 0,\ x = 0$
$C(t, x) = 0,\ t > 0,\ |x| = \infty$

4.3 Discretization and Simulation by Explicit Difference Method

Figure 6 shows a conceptual model for non-steady state diffusion simulation by the explicit difference method. Let consider ΔX and Δt as a thickness in the direction of the depth of bentonite divided equally and a width of time, respectively. Both distance and time step are numbered as shown in **Figure 6**, and each node expresses concentration at a distance and a time step.

The discreted equations for equations (3-2), (4.1-8) and initial and boundary conditions by the explicit difference method are expressed as follows.

Defininig as C(t, x)=Ci, j, equation (3-2) is written as the following difference equations.

$$\frac{C_{i+1,j} - C_{i,j}}{\Delta t} = Da\left(\frac{C_{i,j+1} - C_{i,j}}{\Delta X} - \frac{C_{i,j} - C_{i,j-1}}{\Delta X}\right)\Big/\Delta X$$
$$= Da\left(\frac{C_{i,j+1} - 2C_{i,j} + C_{i,j-1}}{\Delta X^2}\right) \qquad (4.2\text{-}1)$$

We therefore have the following difference equation, arranging equation (4.2-1).

$$C_{i+1,j} = C_{i,j} + Da\frac{\Delta t}{\Delta X^2}\left(C_{i,j+1} - 2C_{i,j} + C_{i,j-1}\right) \qquad (4.2\text{-}2)$$
$$(i = 1, 2, 3, \cdots\cdots, j = 2, 3, 4, \cdots\cdots n_x)$$

Where nx is the number of divisions in the direction of the thickness of bentonite. Where input condition of $Da\cdot\Delta t/\Delta X^2$ in the numerical analysis method adopted in this analysis must be constantly ≤ 1/2 not to cause numerical dispersion [14]. This is due to that rewriting equation (4.2-2) as

$$C_{i+1,j} = \left(1 - 2Da\frac{\Delta t}{\Delta X^2}\right)C_{i,j} + Da\frac{\Delta t}{\Delta X^2}\left(C_{i,j+1} + C_{i,j-1}\right), \qquad (4.2\text{-}3)$$

since $Da \bullet \Delta t/\Delta x^2 > 0$ and $C_{i,j}$, $C_{i,j+1}$ and $C_{i,j-1}$ are also positive, it must be $Da \bullet \Delta t/\Delta x^2 \geq 0$ to be constantly $C_{i+1,j} > 0$.

The relation between ΔX and nx is given by the following equation.

$$n_x = \frac{H}{\Delta X} \qquad (4.2\text{-}4)$$

Where H is the distance long enough, which can be regarded as infinite.

The diffusional mass flux in equation (4.1-8) is discreted as follows.

(at x = 0)

$$J_{i,j} = -Da\left(\frac{C_{i,j+1} - C_{i,j}}{\Delta X}\right) = Da\left(\frac{C_{i,j} - C_{i,j+1}}{\Delta X}\right) \qquad (4.2\text{-}5)$$

$$(i = 1,\ 2,\ 3,\ \cdots\cdots,\ j = 1)$$

(at x = H)

$$J_{i,j} = -Da\left(\frac{C_{i,j} - C_{i,j-1}}{\Delta X}\right) = Da\left(\frac{C_{i,j-1} - C_{i,j}}{\Delta X}\right) \qquad (4.2\text{-}6)$$

$$(i = 1,\ 2,\ 3,\ \cdots\cdots,\ j = n_x + 1)$$

(at 0 < x < H)

$$J_{i,j} = -Da\left(\frac{C_{i,j+1} - C_{i,j-1}}{2\Delta X}\right) = Da\left(\frac{C_{i,j-1} - C_{i,j+1}}{2\Delta X}\right) \qquad (4.2\text{-}7)$$

$$(i = 1,\ 2,\ 3,\ \cdots\cdots,\ j = 2,\ 3,\ \cdots\cdots n_x)$$

Where Ji, j is the diffusional mass flux at the time step and distance (i, j).

The distance from the starting point and the accumulative time, Xj and ti, respectively, are calculated by the following equations.

$ti = (i-1)\cdot\Delta t \qquad (i = 1, 2, 3, \cdots\cdots\cdots\cdots)$

$Xj = (j-1)\cdot\Delta X \qquad (j = 1, 2, 3, \cdots\cdots nx+1)$

Initial and boundary conditions are expressed by the following difference equations.

Initial condition

$Ci, j = 0,\ i = 1,\ j \neq 1$

Boundary condition

$Ci, j = Co,\ i \geq 1,\ j = 1$

$Ci, j = 0,\ i \neq 1,\ j = nx+1$

The concentration profile is calculated as parameters Da and Co, and Da and Co input when total sum of the residuals squared between calculated and measured concentrations is the smallest, were adopted. The calculations were carried out by programming in **Fortran** language.

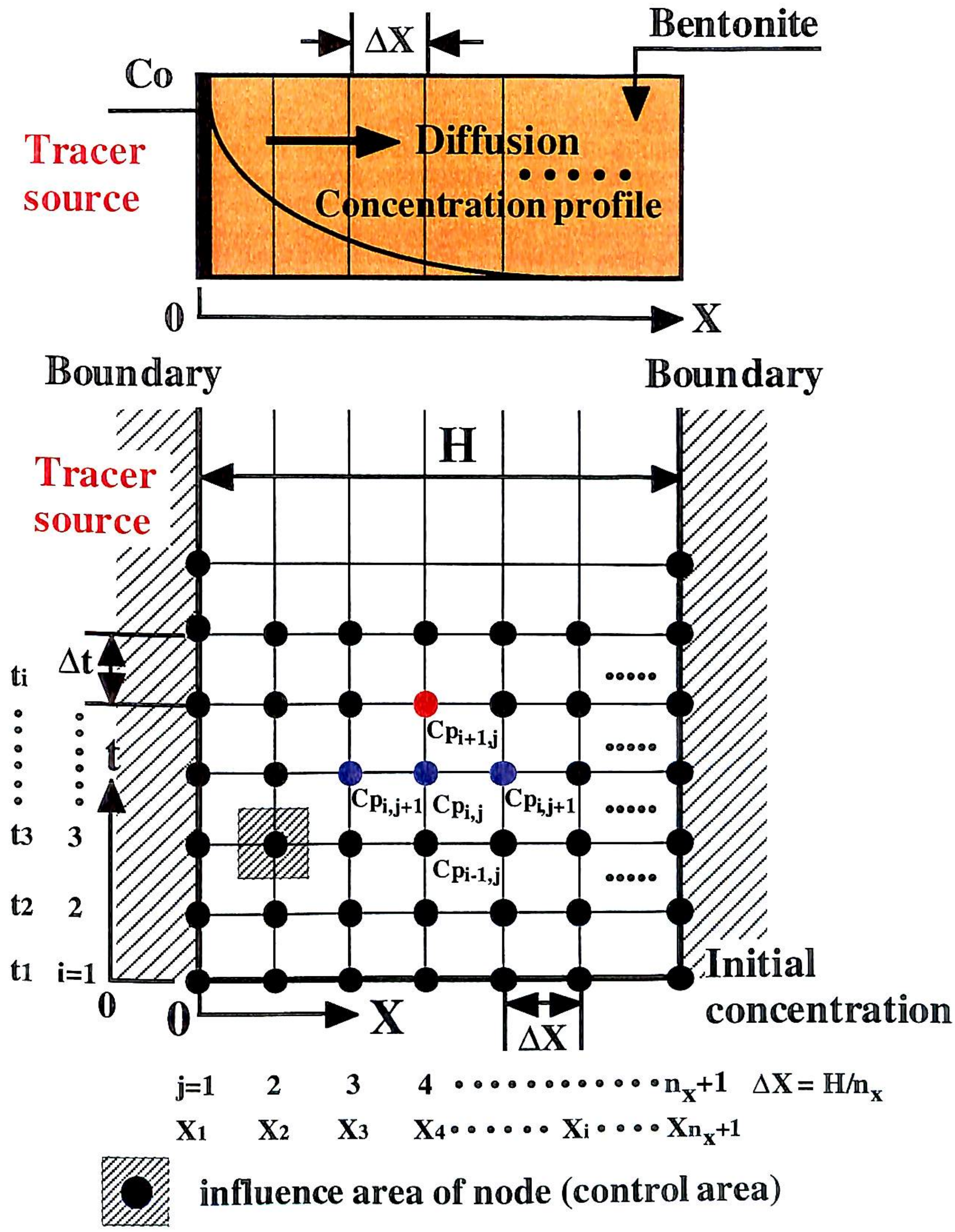

Figure 6 A conceptual model for non-steady state diffusion simulation by explicit difference method

5. RESULTS AND DISCUSSION

5.1 Background of ^{210}Pb in Bentonite

Figures 7(a)–(c) show correlations between total counts per minute (cpm) and depth from the surface of bentonite where tracer was pipetted. Even though slice thickness, bentonite dry density and immersion period are different, no difference in cpm is found and it is approximately constant in a range of 1.87–3.73 cpm over the experimental conditions. Since the differences of slice thickness and bentonite dry density mean the quantity of Pb in bentonite, the obtained results indicate that the effect of ^{210}Pb in bentonite is quite small. **Figure 8** shows cpm measured for a HNO_3 solution used for removal of Pb from bentonite slices with liquid scintillator, a high purity HNO_3 solution (Ultra Analytical Reagent, TAMA CHEMICAL Co., LTD.) with liquid scintillator, liquid scintillator only and an empty polyethylene vial. The cpm values for the HNO_3 solutions with liquid scintillator, liquid scintillator and the empty polyethylene vial were also approximately the same degree as those for bentonite in a range of 1.83–2.93 cpm.

This indicates that the obtained cpm values are neither originated from bentonite nor HNO_3 solutions. Since the similar degree of cpm values were obtained over the experimental conditions for the background measurements, it is clear that obtained cpm values are the mechanical noise from analytical instrument which can not be eliminated. Based on this, the background of the degree of 1.83–3.73 cpm can not be avoided.

In this study, 3.73 cpm which is the highest of the measured background, was used for the calculations of the concentration profiles of ^{210}Pb in bentonite.

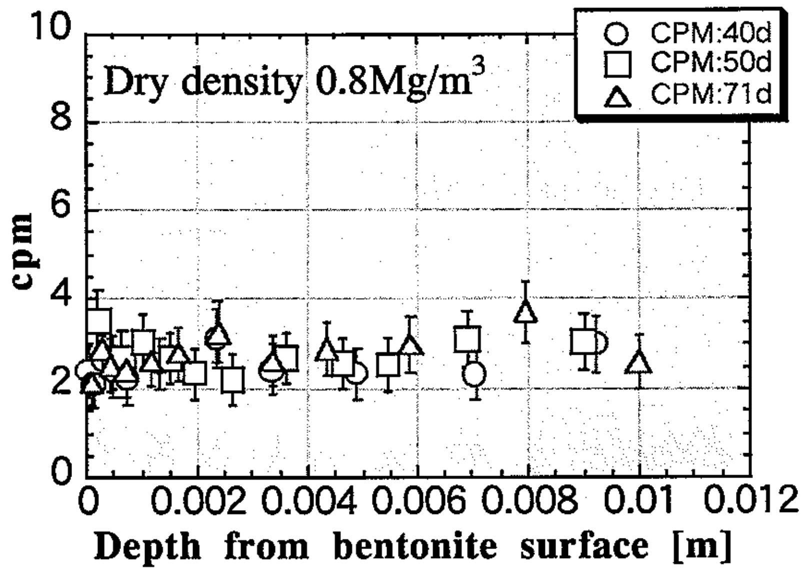

Figure 7(a) Correlations between cpm and depth from bentonite surface at a dry density of 0.8 Mg/m^3 after 40, 50 and 71 days (○: 40 d, □: 50 d, △: 71 d)
The width of error bar shows twice as large as standard deviation.

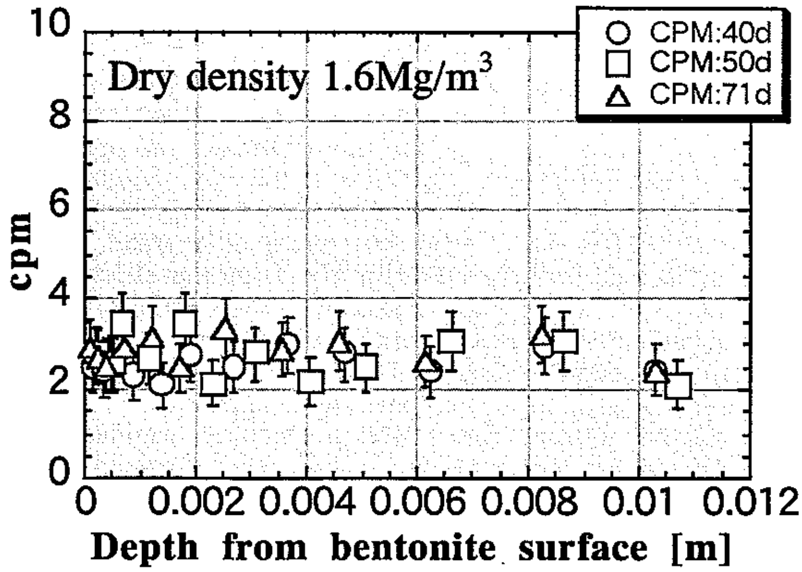

Figure 7(b) Correlations between cpm and depth from bentonite surface at a dry density of 1.6 Mg/m^3 after 40, 50 and 71 days (○: 40 d, □: 50 d, △: 71 d)

The width of error bar shows twice as large as standard deviation.

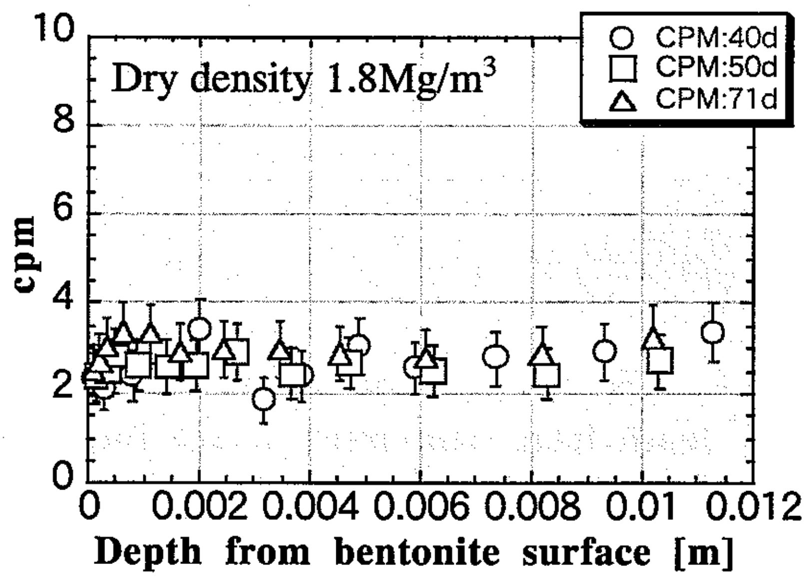

Figure 7(c) Correlations between cpm and depth from bentonite surface at a dry density of 1.8 Mg/m^3 after 40, 50 and 71 days (○: 40 d, □: 50 d, △: 71 d)

The width of error bar shows twice as large as standard deviation.

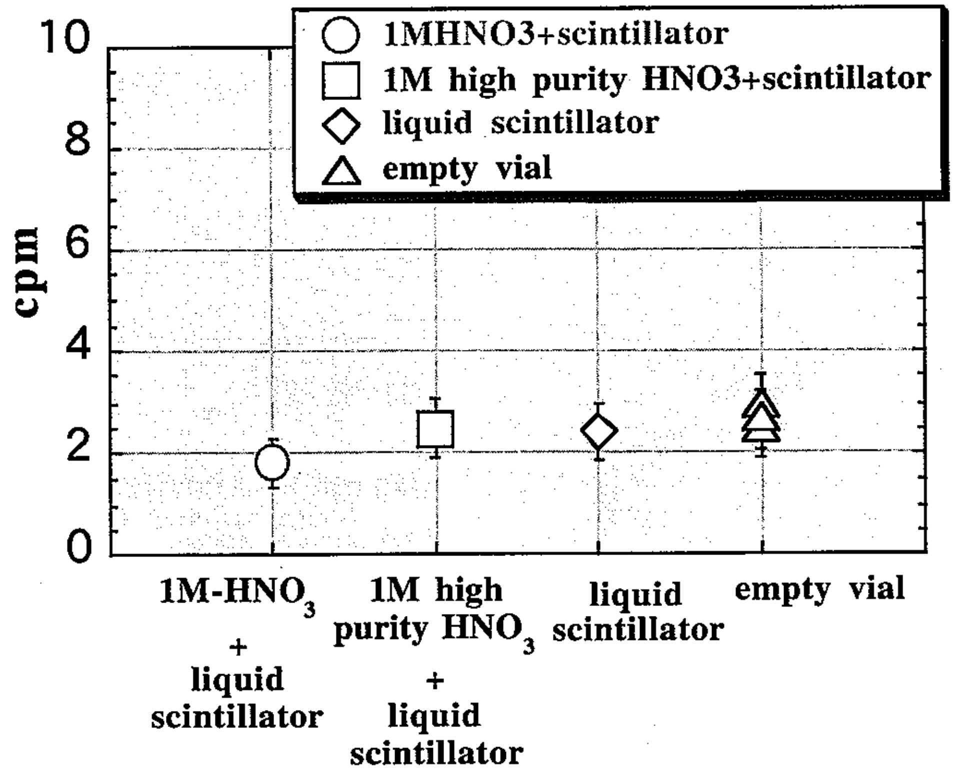

Figure 8 Counts per minute (cpm) for a HNO_3 solution+liquid scintillator, a high purity HNO_3 solution+liquid scintillator, liquid scintillator and an empty polyethylene vial

The width of error bar shows twice as large as standard deviation.

5.2 Detection Efficiency in Analysis of ^{210}Pb, Concentration Profiles of ^{210}Pb in Bentonite and Da Values

Figures 9(a)–(f) show the obtained concentration profiles of ^{210}Pb in bentonite together with fitting curves. The diffusion of ^{210}Pb is quite slow and the distance penetrated in the diffusiong period (78–210 d) was several mm at the maximum for both temperature conditions. The experiment was carried out in duplicate changing diffusing time for the same condition, but concentration profile could not be obtained for short diffusing period (14–27 d), because ^{210}Pb did not penetrate in such short periods. The detection efficiency in analysis by liquid scintillation counter was approximately 95% in this study. As shown in each **Figures 9(a)–(f)**, ^{210}Pb diffused at 60 °C deeper than at room temperature from the surface of bentonite. **Table V** shows a summary of Da values obtained as a function of bentonite dry density, silica sand content and temperature in this study.

The obtained Da values, in a range of 10^{-17} to 10^{-15} m^2/s order at 22.5 °C, decreased with increasing bentonite dry density and showed a tendency to increase with increasing silica sand content in the bentonite and temperature. The Da values obtained at 60 °C were in a range of 10^{-15} to 10^{-14} m^2/s order and showed a tendency to decrease with increasing bentonite dry density, but only Da at 1.8 Mg/m^3 showed a different tendency from the other densities. **Figure 10** shows a dependency of bentonite dry density on Da obtained in this study. The effects of bentonite dry density, silica sand content and of temperature are summarized as follows.

(1) Although Da values increase with increasing temperature, the degree depends on dry density and silica sand content.
(2) Although Da values at room temperature decrease with increasing bentonite dry density, those at 60 °C show a different dependency.
(3) Da values increase with increasing silica sand content.

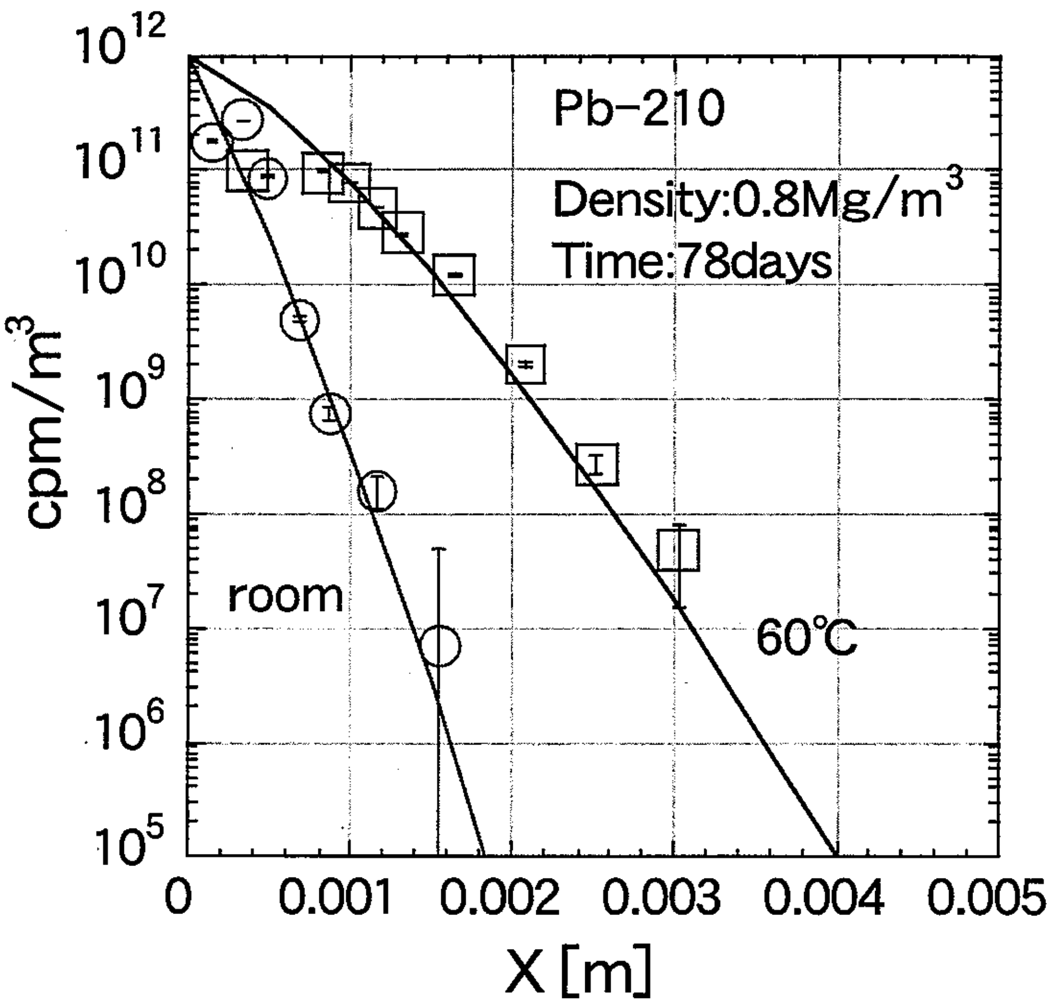

Figure 9(a) Concentration profiles of ^{210}Pb in bentonite and least squares fitting curves at a bentonite dry density of 0.8 Mg/m^3 without silica sand (○: room temperature, □: 60 °C)
The width of error bar shows twice as large as standard deviation.

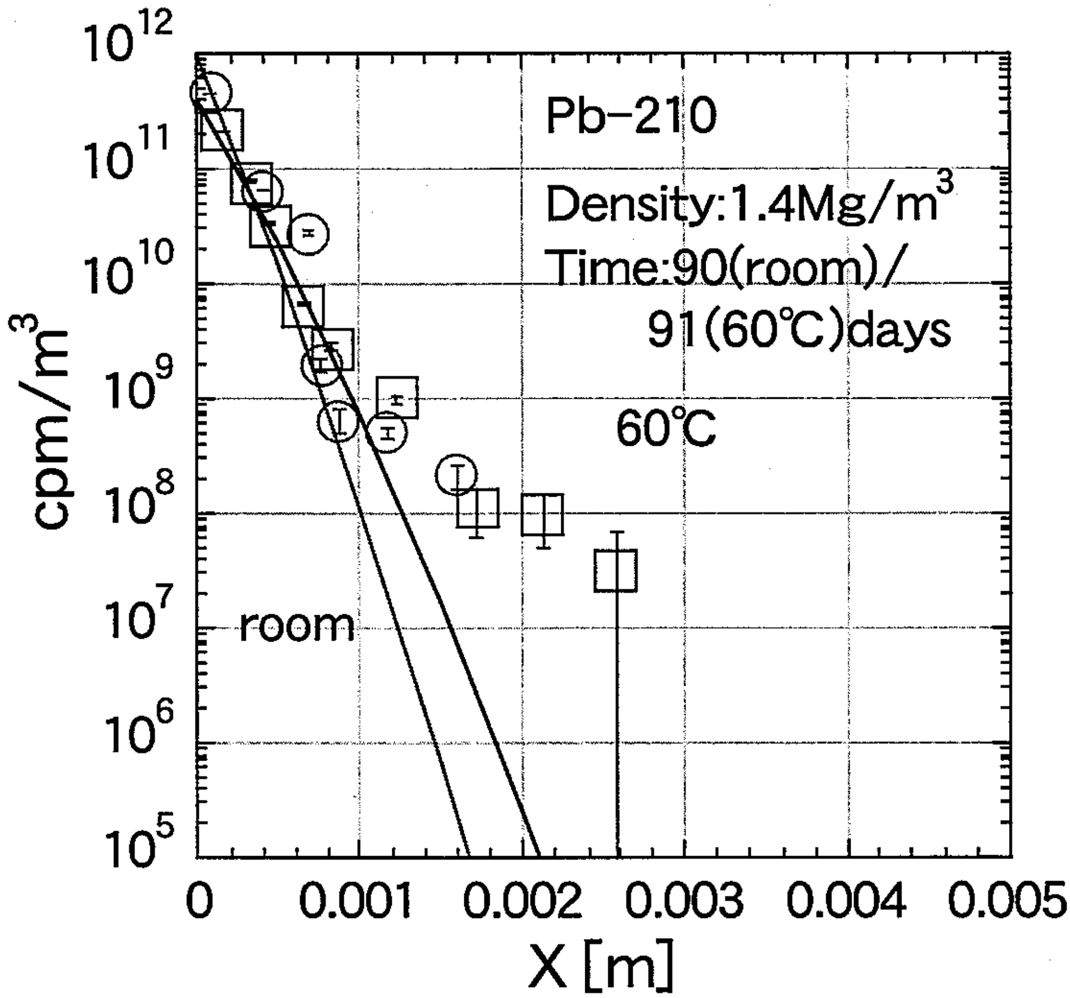

Figure 9(b) Concentration profiles of ^{210}Pb in bentonite and least squares fitting curves at a bentonite dry density of 1.4 Mg/m^3 without silica sand (○: room temperature, □: 60 °C)

The width of error bar shows twice as large as standard deviation.

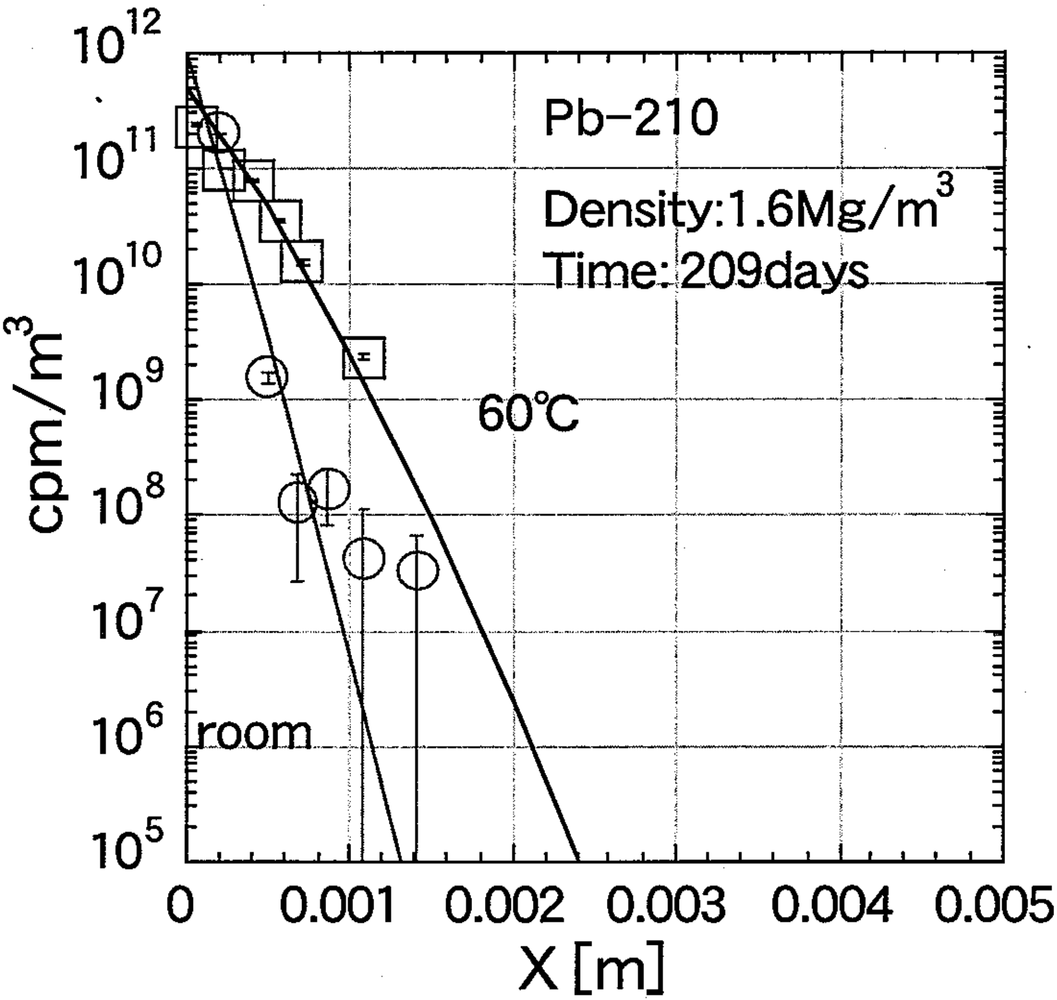

Figure 9(c) Concentration profiles of ^{210}Pb in bentonite and least squares fitting curves at a bentonite dry density of 1.6 Mg/m^3 without silica sand (○: room temperature, □: 60 °C)

The width of error bar shows twice as large as standard deviation.

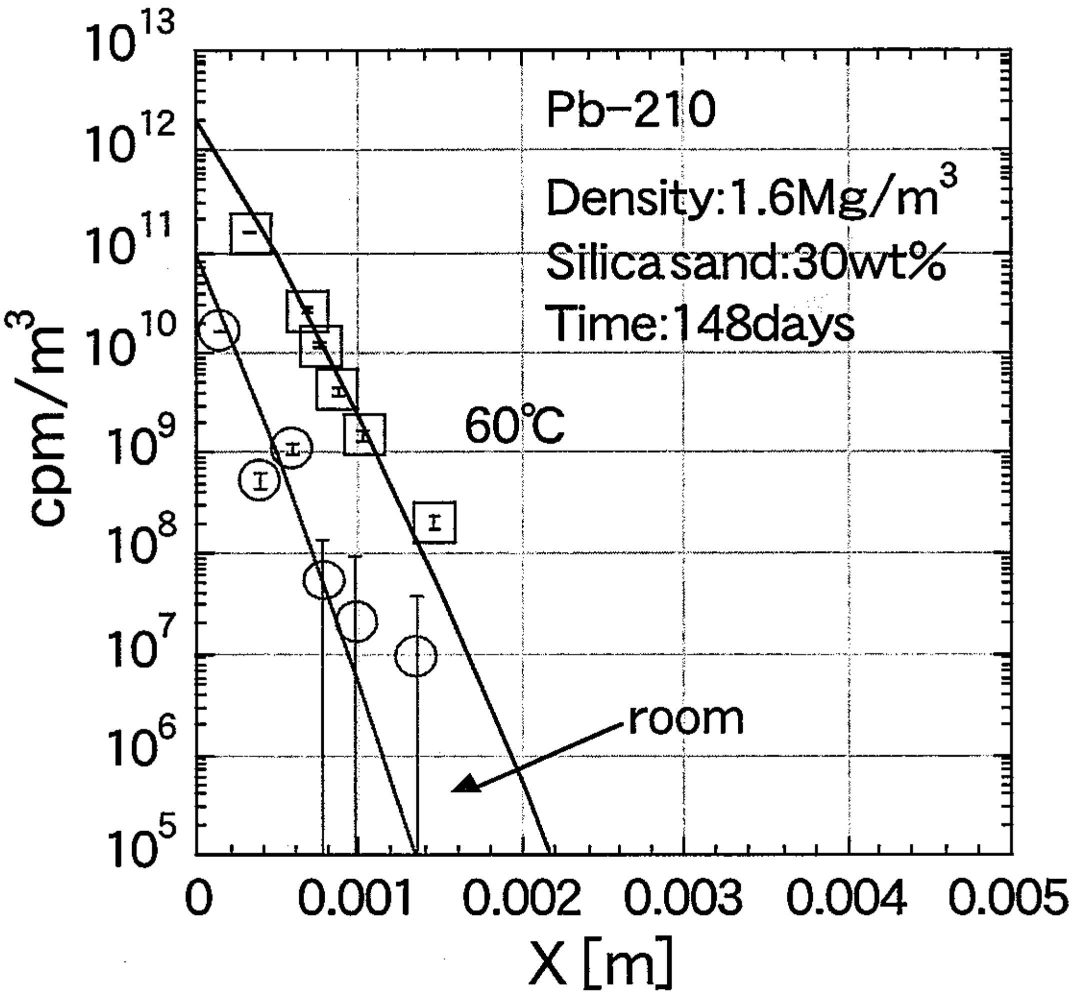

Figure 9(d) Concentration profiles of ^{210}Pb in bentonite and least squares fitting curves at a bentonite dry density of 1.6 Mg/m^3 with silica sand of 30 wt% (○: room temperature, □: 60 °C)
The width of error bar shows twice as large as standard deviation.

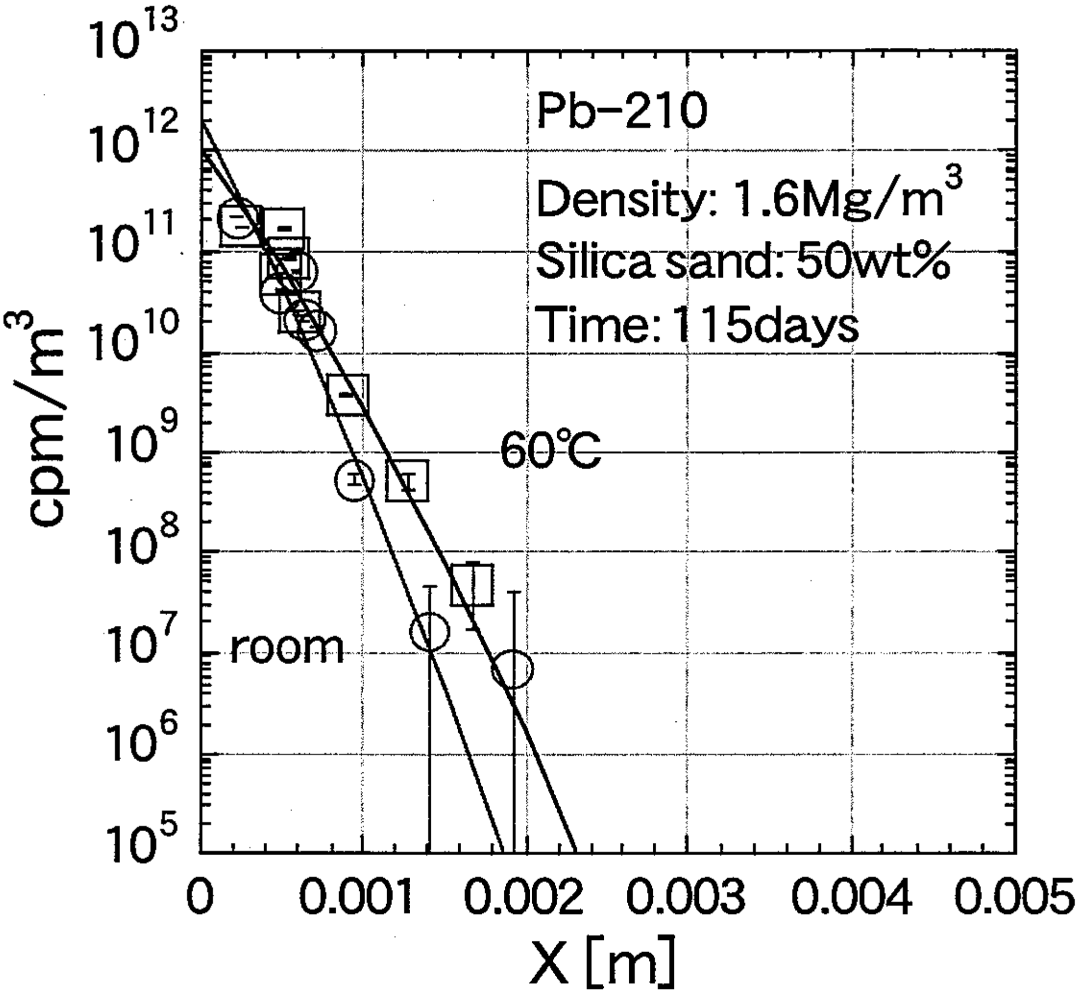

Figure 9(e) Concentration profiles of ^{210}Pb in bentonite and least squares fitting curves at a bentonite dry density of 1.6 Mg/m^3 with silica sand of 50 wt% (○: room temperature, □: 60 °C)
The width of error bar shows twice as large as standard deviation.

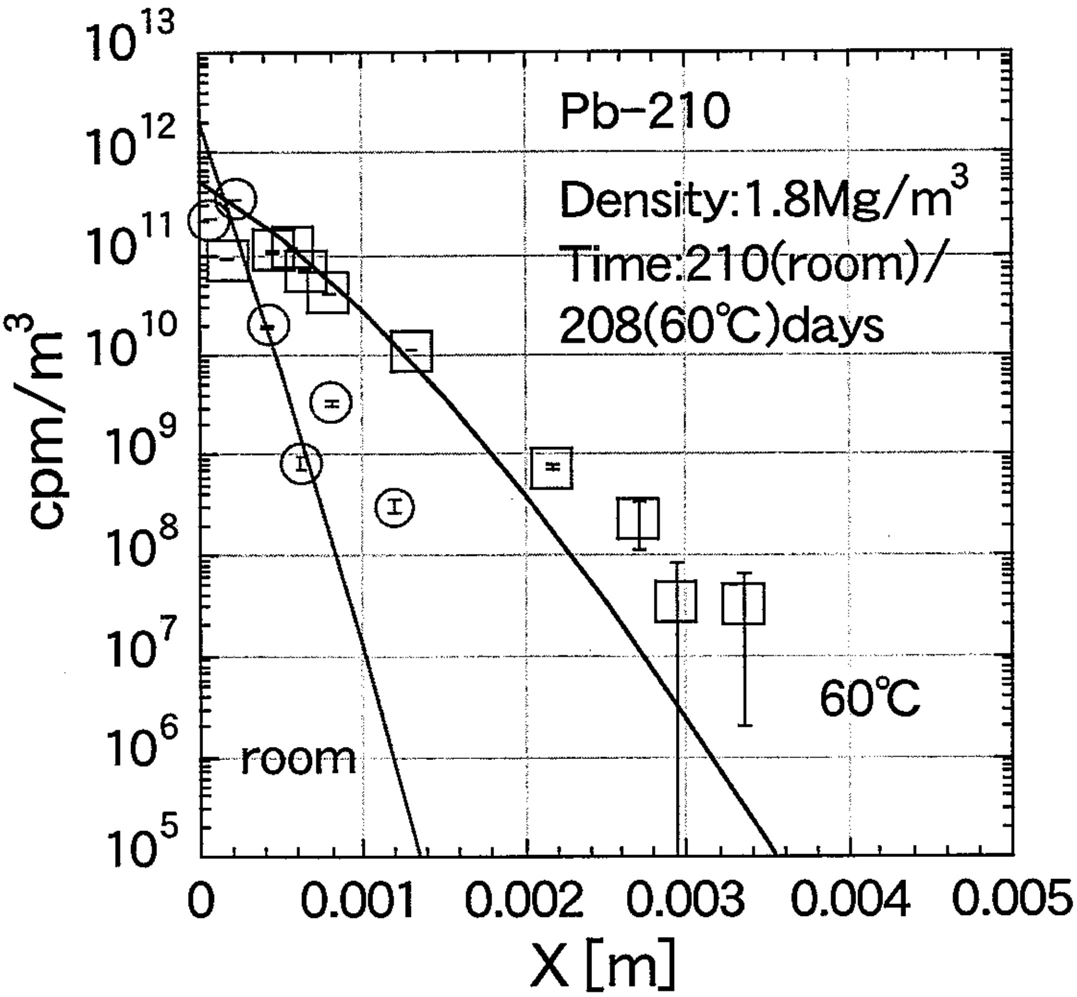

Figure 9(f) Concentration profiles of ^{210}Pb in bentonite and least squares fitting curves at a bentonite dry density of 1.8 Mg/m^3 without silica sand (○: room temperature, □: 60 °C)

The width of error bar shows twice as large as standard deviation.

Table V A summary of Da values obtained as a function of bentonite dry density, silica sand content and temperature

Sample No.	Temperature [°C]	Dry density of bentonite ρ_d [Mg/m^3]	Silica sand content [wt%]	Smectite partial density ρ_{dm} [Mg/m^3]	Time [d]	Da [m^2/s]	Co [cpm/m^3]
2	22.5	0.8	0	0.47	78.0	1.0E-15	1.0E12
4	60	0.8	0	0.47	78.0	2.0E-14	1.0E12
6	22.5	1.4	0	0.95	90.0	5.0E-16	1.0E12
8	60	1.4	0	0.95	91.0	2.0E-15	4.0E11
10	22.5	1.6	0	1.14	209.0	5.0E-17	1.0E12
12	60	1.6	0	1.14	209.0	1.5E-15	5.0E11
14	22.5	1.6	30	0.91	148.0	2.0E-16	1.0E11
16	60	1.6	30	0.91	148.0	1.0E-15	2.0E12
18	22.5	1.6	50	0.72	115.0	6.0E-16	2.0E12
20	60	1.6	50	0.72	115.0	2.0E-15	1.0E12
22	22.5	1.8	0	1.35	210.0	5.0E-17	2.0E12
24	60	1.8	0	1.35	208.0	6.0E-15	5.0E11

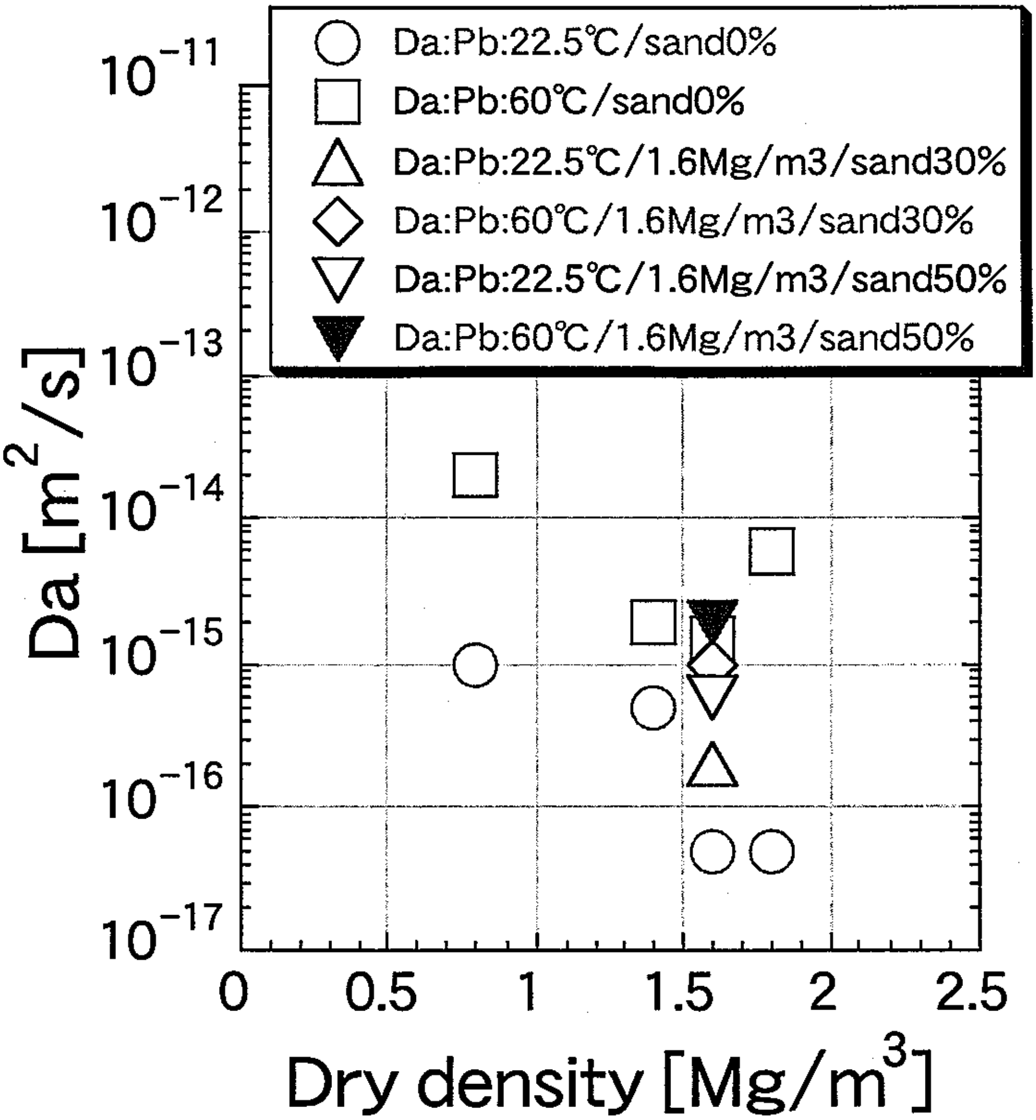

Figure 10 The effects of bentonite dry density, silica sand content and of temperature on Da for ^{210}Pb

The Da values showed a tendency to decrease with increasing dry density of bentonite and to increase with increasing the content of silica sand in bentonite. In addition, Da values increased with a tendency of increase in temperature.

Figure 11 shows dependencies of Da reported to date for various elements in Kunigel-V1® on bentonite dry density (HTO, Fe, Tc, Se, Cs, Np, Zr, Am, Ni, Sm, U, Pu) [15–22] together with data for Pb. The Da values for ^{210}Pb are smaller than those of the other elements. It is quite small compared with data of Ni [19] which chemically takes similar behaviour. With respect to diffusion of Ni in bentonite, Da values quite lower [19] than data previously the authors reported [12] have been also obtained at similar condition and this discrepancy has been concluded to be attributed to the concentration dependency of sorption on bentonite, because a study for equiliblium concentration dependencies of Kd for Ni on Na-montmorillonite at various pH values had been reported [23]. The Da values for ^{210}Pb obtained in this study were further low even though considered those.

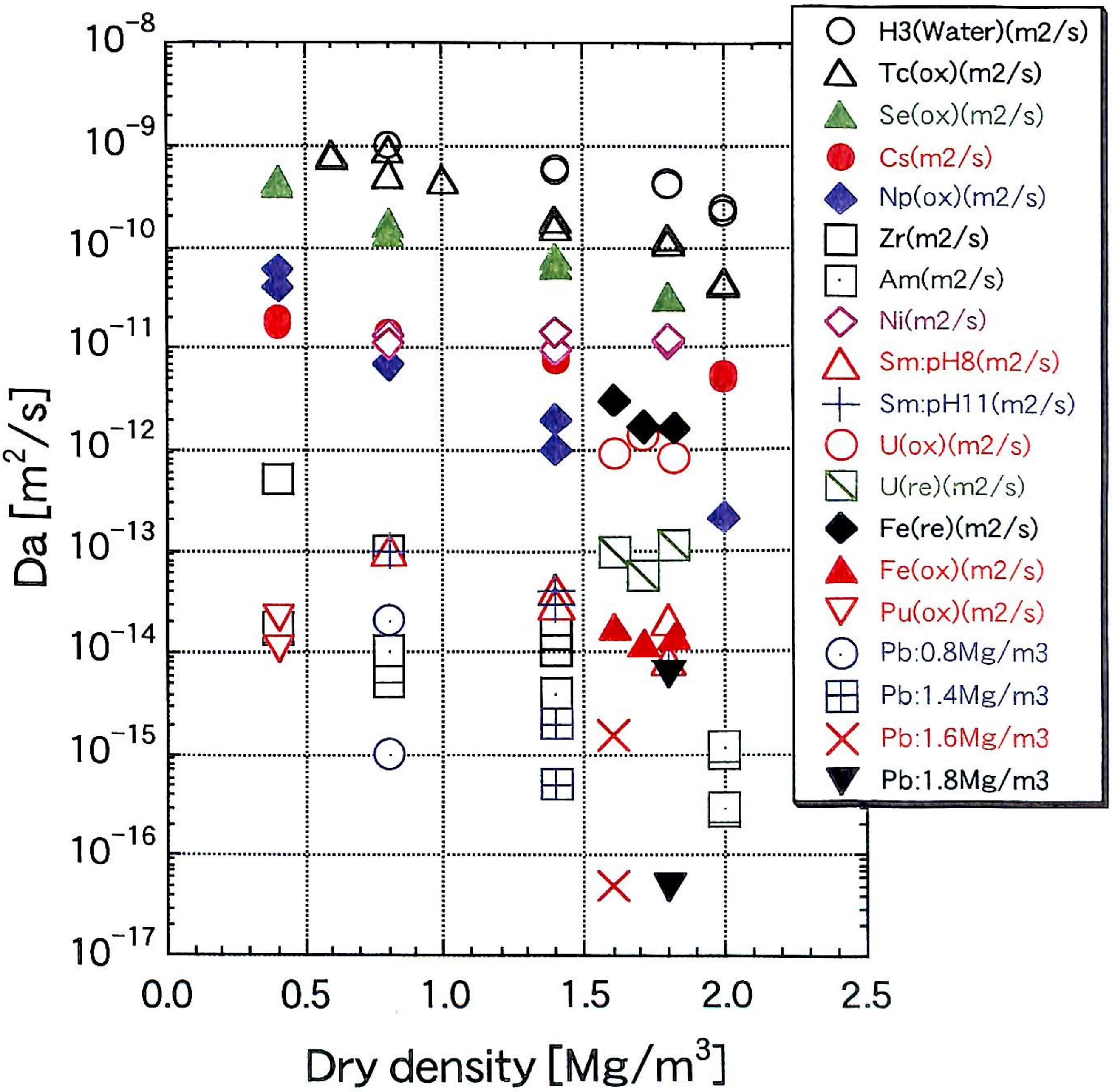

Figure 11 Dependencies of Da for various elements reported to date on bentonite dry density (for Kunigel-V1®)(HTO, Tc, Se(IV), Cs, Np: [15], Zr: [16], Am: [15, 17], Ni: [19], Sm: [18], Fe: [20], U: [21, 22], Pu: [17])

5.3 Correlations between Da Values and Smectite Partial Density

Figure 12 shows an image of the micropore structure for bentonite. Bentonite is composed of smectite which is major clay mineral and impurities such as chalcedony, quartz, plagioclase, calcite, dolomite and pyrite. The detailed mineralogy of bentonite used in this study is described in the literatures [24, 25]. As shown in **Figure 12**, smectite, which is major clay mineral of bentonite, is considered to compensate spaces between impurities. In this case, it is presumed that nuclides diffuse in smectite compensating the spaces between the impurities, because nuclides can not pass through each mineral composing the impurities. It is well known from many literatures reported to date that the diffusion of nuclides in smectite depends on the dry density.

Here we consider a density focused on smectite part only, so called the "smectite partial density". This parameter is the same meaning as montmorillonite density proposed by Kuroda et al. [26]. In the case of Kuroda et al., the montmorillonite density is defined only for Kunigel-V1®, while the smectite partial density, which we defined, is more generalized than that, because the parameter, which we proposed, covers also the montmorillonite density for Kunigel-V1®, which Kuroda et al. proposed [26].

The montmorillonite density, which was defined by Kuroda et al. [26], is given by the following equation.

$$\rho_{dm} = \frac{fm \cdot \rho_d}{1 - \left(\frac{1 - fm}{\rho_{im}} \right) \rho_d} \qquad (5.3\text{-}1)$$

Furthermore, the smectite partial density for a bentonite added silica sand is generally calculated by the following equation (see **appendix 1**: detailed derivation).

$$\rho_{dm} = \frac{(1 - fs) \cdot fm \cdot \rho_d}{1 - \left\{ \frac{(1 - fs)\,(1 - fm)}{\rho_{im}} + \frac{fs}{\rho_s} \right\} \rho_d} \qquad (5.3\text{-}2)$$

Where ρ_{dm} is the smectite partial density (Mg/m^3), ρ_d is the bentonite dry density (Mg/m^3), ρ_{im} is the average pure density of impurities (Mg/m^3), ρ_s is the pure density of silica sand (Mg/m^3), fs is the silica sand content in bentonite (= silica sand weight/(silica sand+bentonite weight))(Mg/Mg), and fm is the smectite content in bentonite (= smectite weight/(smectite+impurities weight)) (Mg/Mg).

With respect to the calculations of ρ_{dm}, a density of 2.7 Mg/m^3 was used for both ρ_{im} and ρ_s in this study. Moreover, fm for Kunigel-V1® was assumed as 0.5 in the calculations of ρ_{dm}. **Figure 13** shows correlations between smectite partial density and bentonite dry density with respect to various kinds of bentonites calculated based on equation (5.3-2). In the calculations, fm values for Kunigel-V1®, Kunipia-F®, MX-80, Avonlea bentonite and Korean bentonite were assumed as 0.5, 1.0, 0.75 [27, 28], 0.8 [29] and 0.87 [30], respectively. Furthermore, the calculated results are shown in **appendix 2**.

The detailed mineralogy of MX-80, Avonlea bentonite and Korean bentonite is described in the literatures [28], [29] and [30], respectively. The MX-80 is a product of the American Colloid Co [27] and its content of montmorillonite is about 75 wt%. In addtion, impurities such as quartz, feldspar and some micas, sulphides and oxides are contained in MX-80 [28]. The Avonlea bentonite is from the Bearpaw Formation of Upper Cretaceous age in southern Saskatchewan, Canada and contains about 80 wt% smectite (montmorillonite), 10 wt% illite, 5 wt% quartz and minor amounts of gypsum, feldspar and carbonate [29]. The Korean bentonite is Ca-bentonite from Younil, Kyungsangbukdo, Korea and consists of 87 wt% montmorillonite and small amounts of feldspar, quartz, zeolite, biotite and Kaolinite [30].

Figure 14 shows a dependency of Da for ^{210}Pb in bentonite on smectite partial density. The Da values decrease with increasing smectite partial density and are well correlative with smectite partial density at room temperature (22.5 °C). On the other hand, Da values once decrease with increasing smectite partial density and increase with increasing smectite partial density at a density of around 0.9 Mg/m^3 at 60 °C. This indicates a possibility of change in diffusion mechanism at a density of around 0.9 Mg/m^3. Further study and discussion are needed.

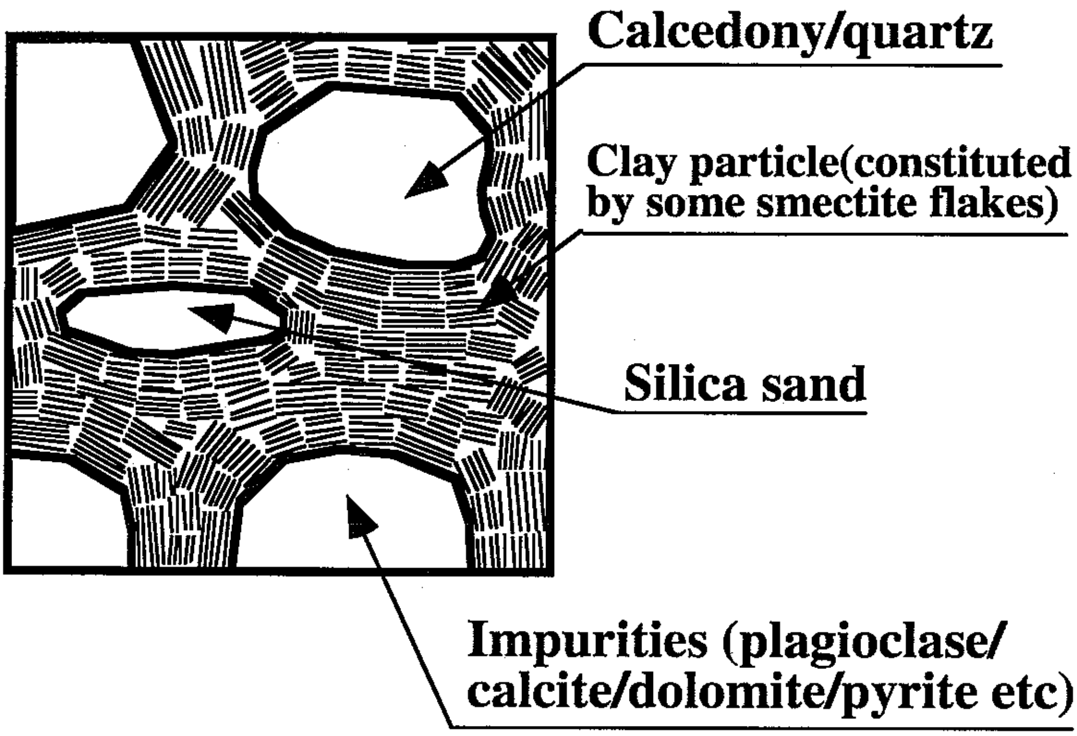

Figure 12 An image of the micropore structure for bentonite (e.g. Kunigel-V1®)

When impurities and added silica sand disperse in bentonite, smectite exists spaces between those impurities and silica sand particles. In this case, smectite partial density is defined by the density in part of smectite only actually contributing for diffusion, because nuclides can diffuse in smectite only. However, the smectite partial density can not express up to passway for diffusion considering the orientation of clay particles.

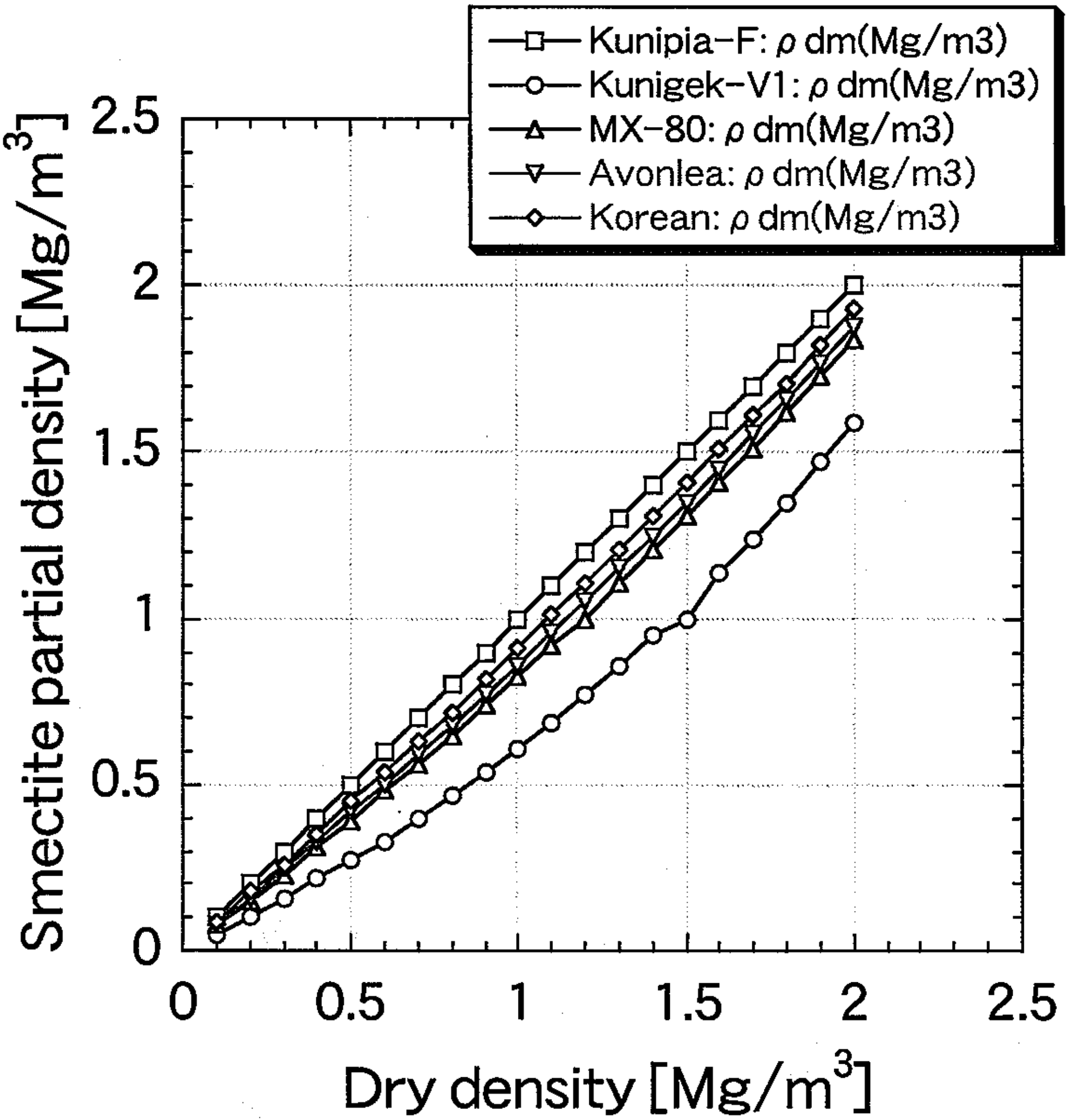

Figure 13 Smectite partial density calculated as a function of dry density with respect to various kinds of bentonites (○: Kunigel-V1®, □: Kunipia-F®, △: MX-80, ▽: Avonlea bentonite, ◇: Korean bentonite)

The contents of smectite for Kunigel-V1®, Kunipia-F®, MX-80, Avonlea bentonite and Korean bentonite were assumed as 0.5, 1.0, 0.75, 0.8 and 0.87 , respectively.

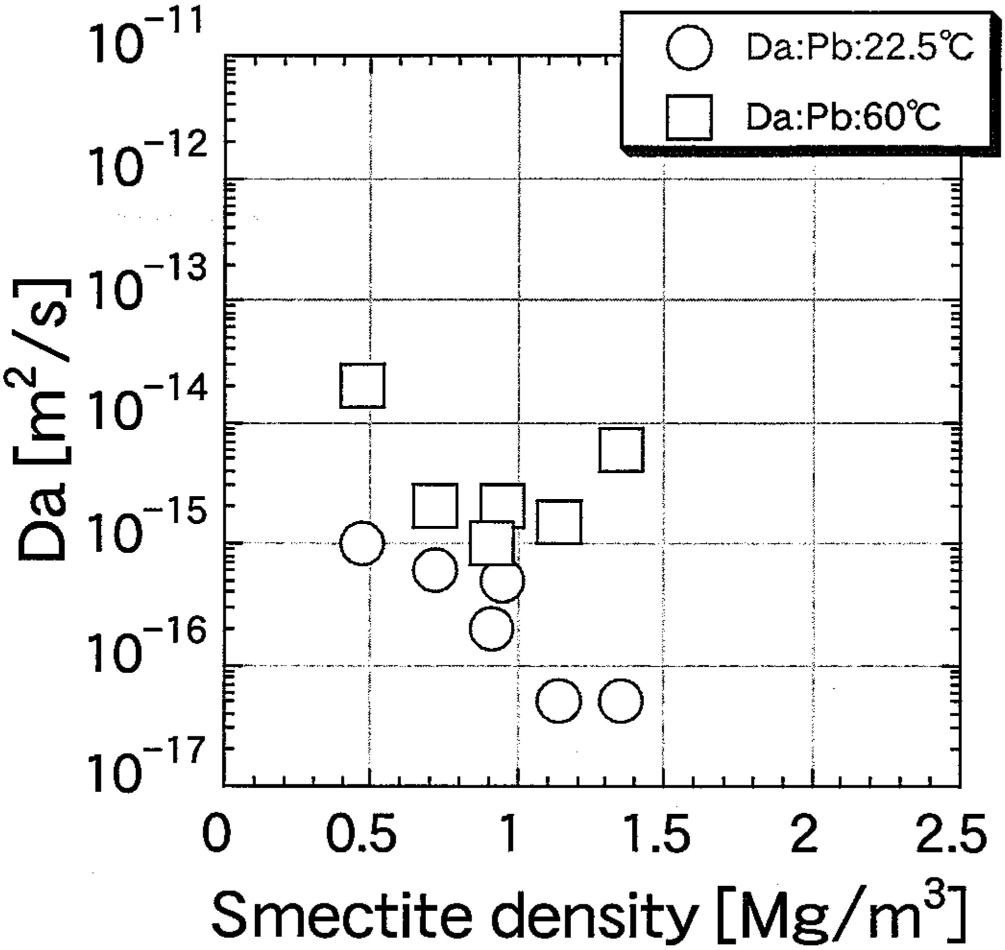

Figure 14 Da values for ^{210}Pb as a function of smectite partial density
The Da values at room temperature uniformally decrease with increasing smectite partial density and are well correlative with smectite partial density, but although those at 60 °C decrease with increasing smectite partial density, those take the smallest value at a density of around 0.9 Mg/m^3 and increase with increasing smectite partial density again.

5.4 The Effect of Temperature on Diffusion and Activation Energy (ΔEa) for Diffusion

Figure 15 shows a dependency of Da of ^{210}Pb at each bentonite dry density on temperature. As shown in **Figure 15**, Da values clearly increase with increasing temperature, but the tendency is different depending on bentonite dry density and silica sand content. The Da values show a tendency to decrease with increasing bentonite dry density. Moreover, Da values show a tendency to increase with increasing silica sand content in bentonite.

Diffusion coefficients for popular ions in free water at 60 °C are about twice as large as those at 25 °C. However, Da values for ^{210}Pb at 60 °C are about one order of magnitude higher than those at room temperature (22.5 °C), showing entirely different temperature dependencies. Since Da includes also retardation by sorption, the dependency of temperature on Kd is also important to understand the effect of temperature on diffusion, especially on Da. However, few studies on temperature dependency of sorption, including Pb have been reported. If there is no dependency of temperature on Kd for Pb, such big gap is considered to be attributed to the limitation of passway for diffusion by the micropore structure of bentonite and to the retardation by that interlayer water and external water between stacks of smectite flakes at compacted state are different from free water.

Activation energies for diffusion (ΔEa) were calculated from temperature dependencies of Da values of ^{210}Pb in bentonite. **Figure 16** shows Da values as a function of the reciprocal number of absolute temperature (1/T), so called the "Arrhenius plot". The relation between Da and temperature is given by the following equations by the Arrhenius plot [31].

$$-\Delta \mathrm{Ea} = \mathrm{R} \cdot \mathrm{T}\ ln\left(\frac{\mathrm{Da}}{\mathrm{D_f}}\right) \qquad (5.4\text{-}1)$$

That is to say,

$$\mathrm{Da} = \mathrm{D_f}\ exp\left(-\frac{\Delta \mathrm{Ea}}{\mathrm{RT}}\right) \qquad (5.4\text{-}2)$$

Figure 17 shows a correlation between ΔEa and smectite partial density. For comparison, ΔEa values of diffusion coefficient in free water for $PbCO_3$(aq) and self-diffusion coefficient in ice for water [32] were also shown in **Figure 17**. The obtained ΔEa values are in a range of 26 to 104 kJ/mol and become the lowest value at a smectite partial density of around 0.9 Mg/m^3. And ΔEa values show a tendency to decrease with increasing silica sand content. Similar tendency that ΔEa values are nearly equal to that for Dw when silica sand was mixed to Na-montmorillonite has been reported also for diffusion of Na^+ ion in compacted Na-montmorillonite [33]. However, a ΔEa of 104 kJ/mol is quite high also compared with that (56.4 and 65.6 kJ/mol) for self-diffusion coefficient in ice.

Thereon, ΔEa of Dw for Pb was calculated and compared with ΔEa data obtained in this study. The dominant species of Pb in the porewater of bentonite is predicted to be $PbCO_3$(aq) [1, 5]. However, no Dw of $PbCO_3$(aq) has been reported to date. Thereon, the Dw for $PbCO_3$(aq) was calculated based on an expression due to the Nernst [34] as shown as follows.

$$\mathrm{D^o} = \frac{(|Z_+| + |Z_-|)\mathrm{D^o}_+ \cdot \mathrm{D^o}_-}{|Z_+|\mathrm{D^o}_+ + |Z_-|\mathrm{D^o}_-} \qquad (5.4\text{-}3)$$

Where D^o is the salt diffusion coefficient at infinite dilution (m^2/s), $|Z_+|$ and $|Z_-|$ are the absolute value of the charge of the respective ions (–), and D^o_+ and D^o_- are the tracer or self-diffusion coefficients of the respective ions at infinite dilution (m^2/s).

The D^o_+ and D^o_- are calculated by the following equation based on the Nernst expression.

$$D^o_\pm = \frac{R \cdot T \cdot \Lambda_\pm}{F^2 \, |Z_\pm|} \qquad (5.3\text{-}4)$$

Where $\Lambda\pm$ is the limiting ionic equivalent conductivity ($m^2 \cdot S/mol$), and F is the Faraday constant (96493 Coulombs/mol).

Lead carbonate ($PbCO_3(aq)$) is dissociated into Pb^{2+} and CO_3^{2-} ions. Since D^o_+ and D^o_- for Pb^{2+} and CO_3^{2-} at 0, 18 and 25 °C are respectively already known, the D^o for $PbCO_3(aq)$, D^o_{PbCO3} was calculated at each temperature by substituting D^o_+ and D^o_- for Pb^{2+} and CO_3^{2-} ions into equation (5.4-3), respectively. Consequently, the ΔEa for D^o_{PbCO3} was calculated to be 20.3 kJ/mol. This ΔEa is lower than those (26–104 kJ/mol) of Da values for ^{210}Pb obtained from diffusion experiments in this study. However, ΔEa values for Da values in compacted montmorillonite added silica sand are approximately the same over the montmorillonite partial densities [33].

The author has experimentally investigated diffusion direction dependency to compacted direction on De using tritiated water (HTO) which is a non-sorbing nuclide on bentonite through Kunipia-F® and Kunigel-V1® at bentonite dry densities of 1.0 and 1.5 Mg/m^3 [35]. Through-diffusion experiments were carried out for 2 kinds of diffusion directions to compacted direction, axial and perpendicular directions to compacted direction for Kunigel-V1® and Kunipia-F®. In addition, scanning electron microscope (SEM) observations for the cross section of sample to axial and perpendicular directions to compacted direction were also carried out to discuss the effect of clay particle orientation on De. Consequently, the results of SEM observations showed that no significant orientation of clay particle was found for Kunigel-V1® over the densities. On the other hand, the orientation of clay particle was clearly found for Kunipia-F®. **Figures 18 (a)–(c)** show cross-sectional photographs by SEM for Kunigel-V1® and Kunipia-F® at dry densities of 1.0, 1.6 and 2.0 Mg/m^3, which were saturated with synthetic porewater after being compacted. The chemical composition of the synthetic porewater and detailed procedure for the preparation of sample are described in the literature [36]. The bentonite samples were prepared by the following procedure.

(1) The filling of bentonite powder dried 24 h at 50 °C into a diffusion column to obtain desired densities (1.0, 1.6, 2.0 Mg/m^3).
(2) The saturation of bentonite with synthetic porewater.
(3) Pushing out of the cylindrical bentonite from the column, freezing in liquid nitrogen and drying in a vacuum chamber.
(4) Cutting of the bentonite in the axial and perpendicular directions to compacted direction.
(5) SEM observations for both directions (magnification: 200 times).

This effect by the difference in the orientation of clay particle was found also with respect to De values for both bentonites. The De values of HTO for perpendicular direction to compacted direction were several times as large as those for axial direction to compacted direction for Kunipia-F®. However, De values of HTO for both diffusion directions for Kunigel-V1® were approximately the same over the densities. Therefore, discrepancy of ΔEa for Da values between montmorillonite and montmorillonite added silica sand is considered to be attributed to the difference of the orientation property of clay particle.

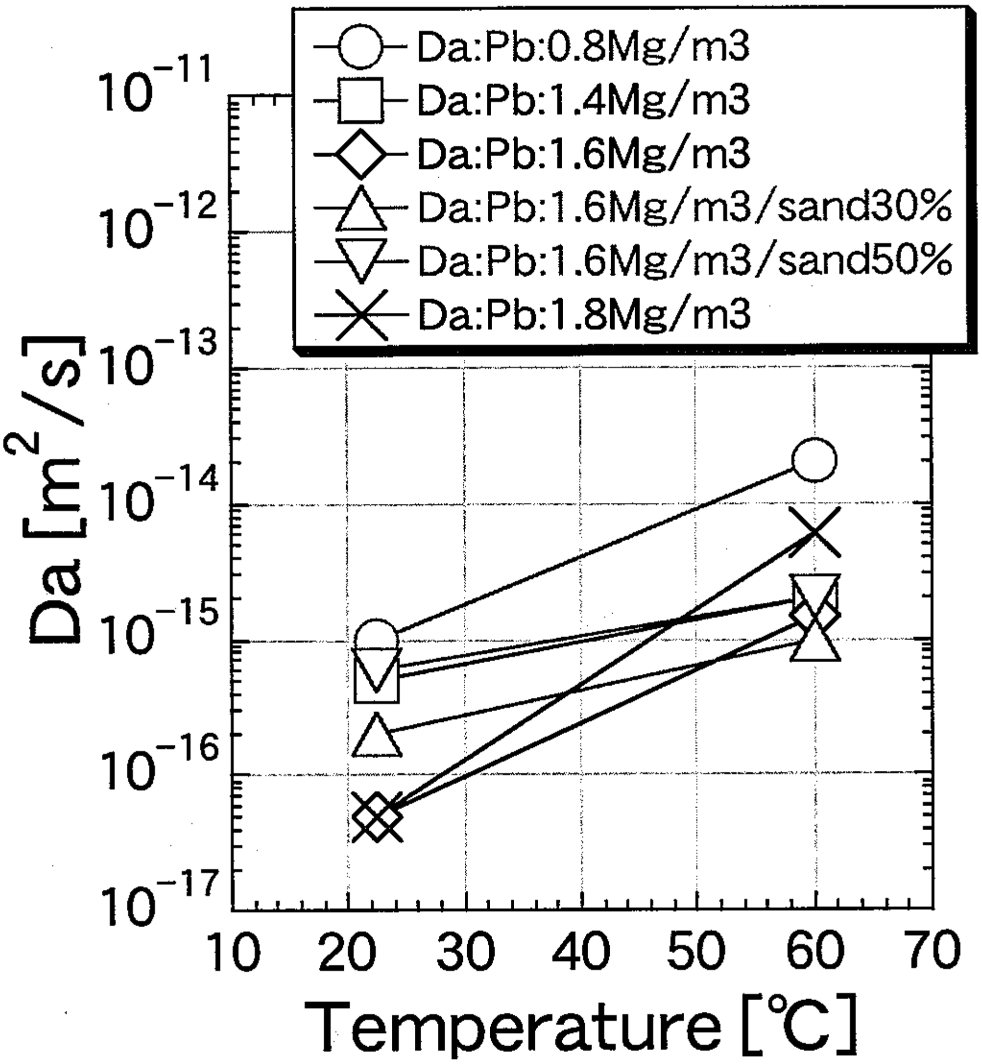

Figure 15 Da values of ^{210}Pb in bentonite as a function of temperature and bentonite dry density

All Da values at 60 °C are higher than those at room temperature.

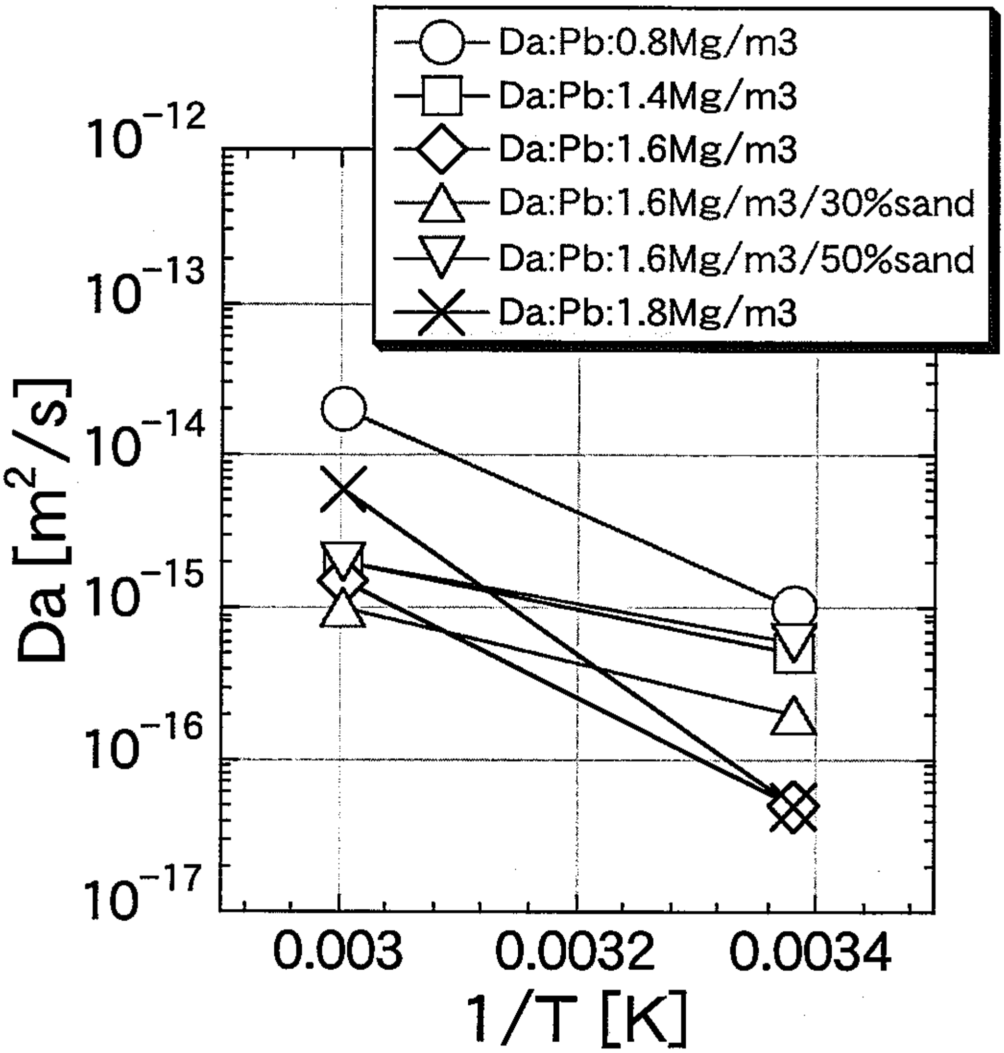

Figure 16 Da values as a function of the reciprocal number of absolute temperature (1/T)(Arrhenius plot)

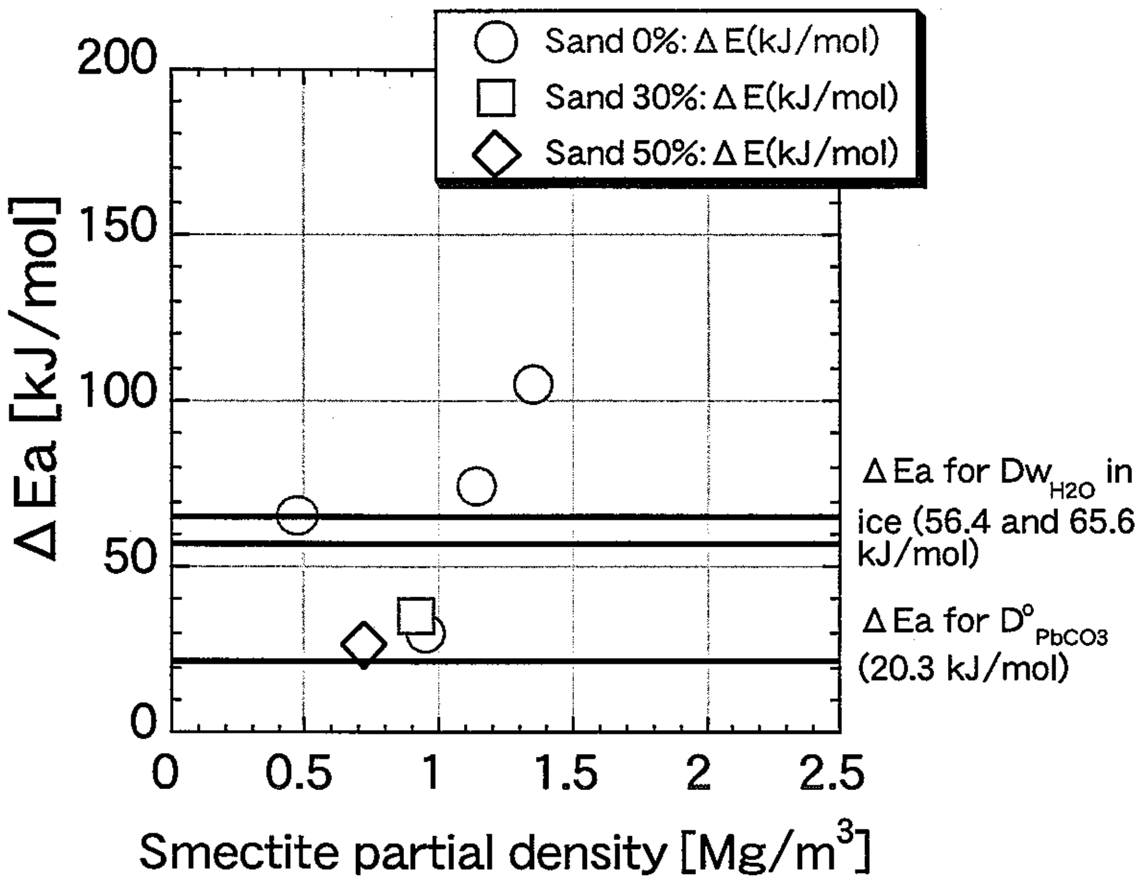

Figure 17 A correlation between ΔEa and smectite partial density
The ΔEa takes the lowest value at a dry density of around 0.9 Mg/m^3. The bold lines shown in the figure show ΔEa values of diffusion coefficient in free water for $PbCO_3$(aq) and self-diffusion coefficient in ice for water, respectively.

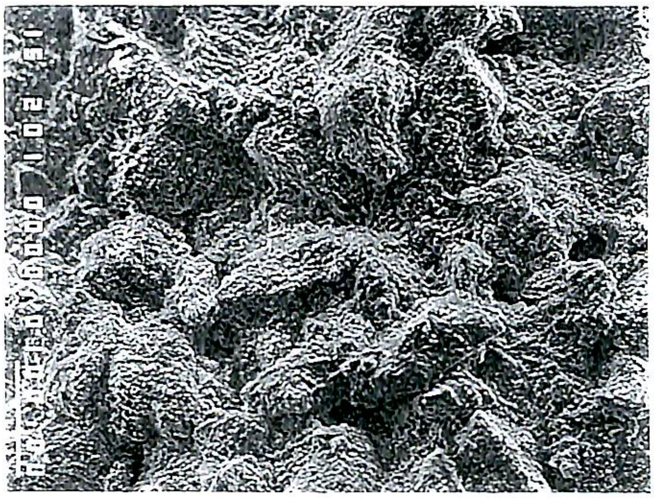

Photograph (a)-1

Photograph (a)-3

Photograph (a)-2

Photograph (a)-4

Figure 18(a) Cross-sectional photographs by SEM for Kunigel-V1® and Kunipia-F® at a dry density of 1.0 Mg/m^3

(a)-1 and (a)-2: cross-sectional photographs with respect to perpendicular and axial directions to compacted direction for Kunigel-V1, respectively. (a)-3 and (a)-4: cross-sectional photographs with respect to perpendicular and axial directions to compacted direction for Kunipia-F, respectively.

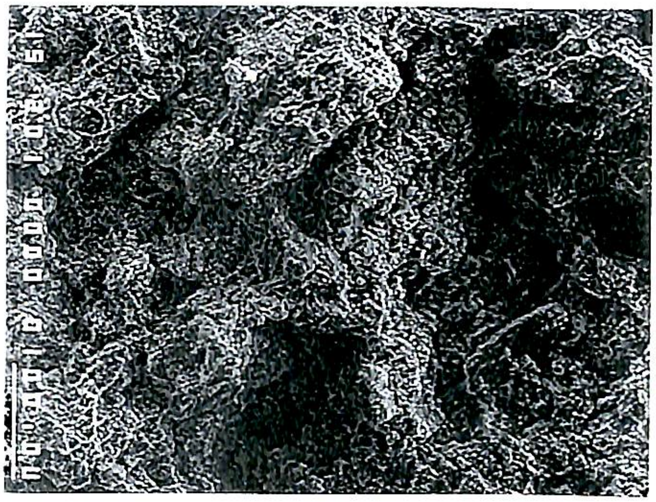

Photograph (b)-1

Photograph (b)-3

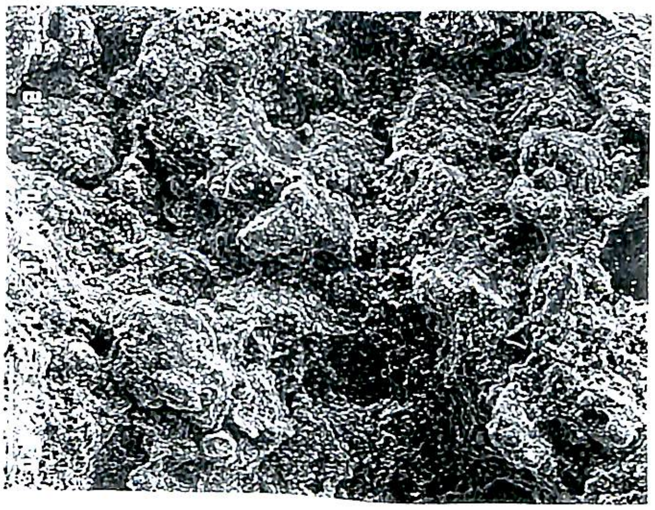

Photograph (b)-2

Photograph (b)-4

Figure 18(b) Cross-sectional photographs by SEM for Kunigel-V1® and Kunipia-F® at a dry density of 1.6 Mg/m^3

(b)-1 and (b)-2: cross-sectional photographs with respect to perpendicular and axial directions to compacted direction for Kunigel-V1, respectively. (b)-3 and (b)-4: cross-sectional photographs with respect to perpendicular and axial directions to compacted direction for Kunipia-F, respectively.

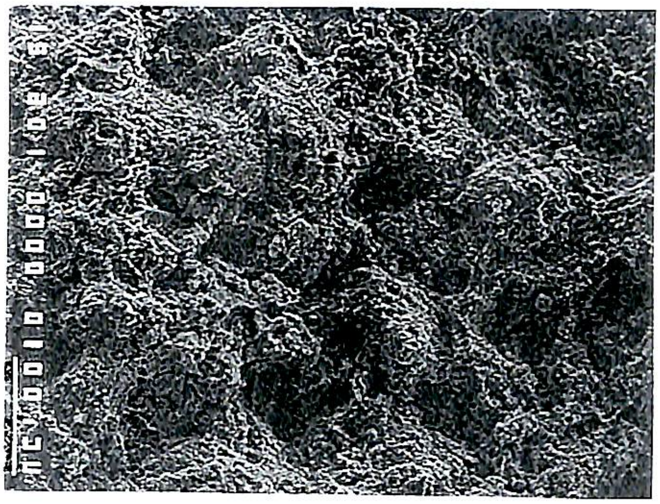

Photograph (c)-1

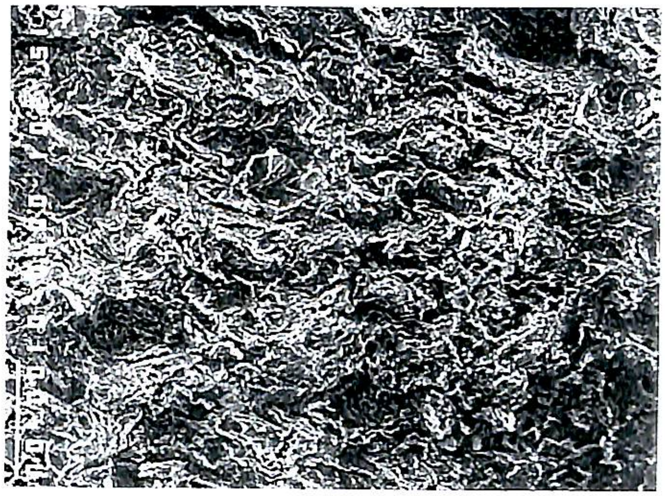

Photograph (c)-3

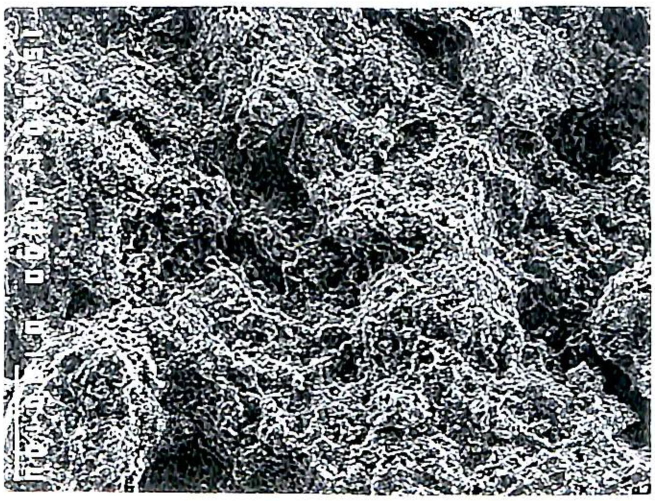

Photograph (c)-2

Photograph (c)-4

Figure 18(c) Cross-sectional photographs by SEM for Kunigel-V1® and Kunipia-F® at a dry density of 2.0 Mg/m^3

(c)-1 and (c)-2: cross-sectional photographs with respect to perpendicular and axial directions to compacted direction for Kunigel-V1, respectively. (c)-3 and (c)-4: cross-sectional photographs with respect to perpendicular and axial directions to compacted direction for Kunipia-F, respectively.

5.5 The Conservativity of Kd for Pb Used in the Second Progress Report

The conservativity of Kd for Pb used for the reference case in the second progress report [1] was discussed. In the second progress report, Kd was determined as follows based on the relation between Kd, Da and De.

$$Da = \frac{De}{\varepsilon + (1-\varepsilon)\,\rho_{ds} \cdot Kd} = \frac{De}{\varepsilon + \rho_d \cdot Kd} \qquad (5.5\text{-}1)$$

Therefore, Kd is calculated as follows.

$$Kd = \frac{1}{\rho_d}\left(\frac{De}{Da} - \varepsilon\right) \qquad (5.5\text{-}2)$$

Where ρ_{ds} is the pure density of bentonite (Mg/m^3), being 2.7 Mg/m^3 for Kunigel-V1® [37].

The porosity, ε is theoretically calculated by the following relation.

$$\varepsilon = 1 - \frac{\rho_d}{\rho_{ds}} \qquad (5.5\text{-}3)$$

Table VI shows each parameter for the reference case in the second progress report. The Kd calculated from Da and De based on equation (5.5-2) was 187.5 m^3/kg, being quite large compared with Kd (0.1 m^3/kg) used in the second progress report. Based on this, the conservativity of Kd for Pb used for the reference case in the second progress report was confirmed.

Table VI Each parameter for the reference case in the second progress report

Bentonite	Kunigel-V1®
Dry density	1.6 Mg/m^3 (porosity $\varepsilon = 0.41$)
Silica sand content	30 wt%
Porewater	FRHP (Fresh-Reducing-High pH) groundwater
Da	1.0E-15 m^2/s (60 °C: measured data in this work)
De	3.0E-10 m^2/s (60 °C: value determined for elements except for Cs and Se)

5.6 Comparisons between Kd Values Calculated from Da Values and Those Obtained by Batch Experiments

With respect to Pb, Kd values on bentonite (Kunigel-V1®) obtained by batch method have been reprted by Tachi [38]. The Kd values have been measured as a function of ionic strength at room temperature and a Kd of about 10^2 m^3/kg has been obtained at 0.01 M NaCl. Thereon, Kd values were calculated from Da values for Pb obtained in this study and De values (De_{PbCO3}) which were determined from De values for HTO (De_{HTO}), D^o_{PbCO3} and Dw for HTO (Dw_{HTO}) and were compared with Kd obtained by batch method. In this case, De_{PbCO3} was determined by the following equation.

$$De_{PbCO3} = \left(\frac{D^o{}_{PbCO3}}{Dw_{HTO}} \right) De_{HTO} \qquad (5.6\text{-}1)$$

Where De_{PbCO3} is the effective diffusion coefficient for $PbCO_3$(aq) (m^2/s), D^o_{PbCO3} is the diffusion coefficient at infinite dilution for $PbCO_3$(aq) (= 9.5×10^{-10} m^2/s at 25 °C), Dw_{HTO} is the self-diffusion coefficient in free water for HTO (m^2/s) (= 2.14×10^{-9} m^2/s at 25 °C [39]), and De_{HTO} is the effective diffusion coefficient for HTO (m^2/s [15, 38]). The De_{HTO} values were determined from the empirical equation $De_{HTO} = 4.53E{-}9 \bullet exp(-2.27 \bullet \rho_d)$, which the authors derived based on De data for HTO as a function of dry density of bentonite reported by Sato et al. [15] and Kato et al. [40].

The Kd values for Pb were calculated by equation (5.5-2). **Figure 19** and **Table VII** show Kd values calculated from Da and De at each dry density of bentonite.

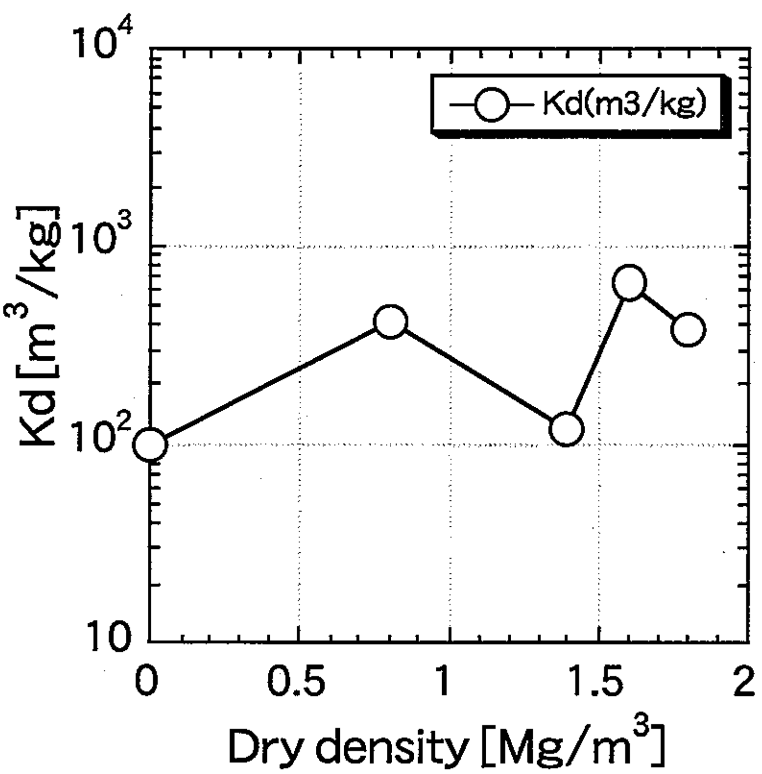

Figure 19 Kd values calculated from Da and De at each dry density of bentonite
The plot on the vertical line shows average Kd obtained by batch experiments.

Table VII Kd values calculated at each dry density of bentonite

Dry density of bentonite ρ_d [m^2/s]	Porosity ε [–]	De_{HTO} [m^2/s]*	De_{PbCO3} [m^2/s]	De_{PbCO3} [m^2/s]	Kd [m^3/kg]
0.8	0.70	7.36E-10	3.27E-10	1.0E-15	408.7
1.4	0.48	1.88E-10	8.35E-11	5.0E-16	119.3
1.6	0.41	1.19E-10	5.28E-11	5.0E-17	660.0
1.8	0.33	7.59E-11	3.37E-11	5.0E-17	374.4

* The effective diffusivities for HTO, De_{HTO} were determined by the following empirical equation which the authors derived based on De data for HTO reported by Sato et al. [15] and Kato et al. [40].

$De_{HTO} = 4.53 \times 10^{-9} \cdot exp(-2.27 \cdot \rho_d)$

r = 0.98276

The plot on the vertical line shows average Kd obtained by batch experiments. The Kd values calculated from Da and De values are little higher than that obtained by batch method on the whole, but those are the same order. This discrepancy between Kd obtained by batch method and those calculated from Da and De values may be attributed to discrepancy between chemical and physical conditions in both batch and diffusion experiments. The cause of discrepancy is open question at the present.

6. CONCLUSIONS

The Da values of Pb in compacted sodium bentonite, which is a candidate buffer material, were obtained as a function of bentonite dry density, silica sand content and temperature using ^{210}Pb as a tracer by in-diffusion method to confirm the validity or conservativity of Kd on the bentonite and to make progress in additional data accumulation as a link in the chain of a follow-up of the second progress report. The conclusion is summarized as follows.

(1) The obtained Da values, in a range of 10^{-17} to 10^{-15} m^2/s order at 22.5 °C, decreased with increasing bentonite dry density and showed a tendency to increase with increasing silica sand content and temperature. The Da values at 60 °C were in a range of 10^{-15} to 10^{-14} m^2/s order and showed a tendency to decrease with increasing bentonite dry density, but only Da at 1.8 Mg/m^3 showed a different tendency from the other densities.
(2) The Da values decreased with increasing smectite partial density and were well correlative with smectite partial density at room temperature. On the other hand, Da values at 60 °C once decreased with increasing smectite partial density and increased with increasing smectite partial density at a density of around 0.9 Mg/m^3.
(3) The calculated ΔEa values are in a range of 26 to 104 kJ/mol and became the lowest value at a smectite partial density of around 0.9 Mg/m^3. And ΔEa values showed a tendency to decrease with increasing silica sand content. Although further study and discussion are needed, it was approximately indicated that Pb was predominantly controlled by the properties in part of smectite.
(4) The conservativity of Kd for Pb used for the reference case in the second progress report was confirmed from comparison between Kd calculated from Da and that used in the second progress report.

7. FUTURE WORK

Some future studies to be solved were extracted through this study. The future study is summarized as follows.

(1) Although Da values decreased with increasing smectite partial density and were well correlative with smectite partial density at room temperature, Da values at 60 °C showed a different tendency in smectite partial density from those at room temperature. Although this indicates a possibility of change in diffusion mechanism, further study and discussion are needed including temperature dependency of sorption.
(2) The obtained ΔEa values were also relatively high between 26 and 104 kJ/mol. The ΔEa values additionally showed a tendency to decrease with increasing smectite partial density and became the lowest value, which was nearly equal to ΔEa for D^{o}_{PbCO3} (20.3 kJ/mol) at a smectite partial density of around 0.9 Mg/m^3. The ΔEa values then increased with increasing smectite partial density again. This may be concerned with the orientation property of clay particle and further discussion with respect to correlation between ΔEa and the orientation of clay particle.
(3) It is general that Kd obtained by batch method does not agree with that calculated from Da and De and such discrepancy in Kd was found also in this study. This is called the "inconsistency of batch-compacted system" and is quite important problem. This is open question to be solved at the present.

8. ACKNOWLEGEMENTS

The authors would like to thank Mr. Minoru Akagi of the Inspection Development

Company (IDC) for analyses of our samples with a liquid scintillation counter. And Mr. Tsutomu Tomura of the IDC is also thanked for supporting in diffusion experiments. We would like to appreciate them very much and to express our attitude describing their names here.

9. REFERENCES

1. Japan Nuclear Cycle Development Institute: "Second Progress Report on Research and Development for the Geological Disposal of HLW in Japan –H12: Project to Establish the Scientific and Technical Basis for HLW Disposal in Japan: Project Overview Report–", JNC TN1410 2000-001 (2000).
2. M. Yui, J. Azuma, and M. Shibata: "JNC Thermodynamic Database for Performance Assessment of High-level Radioactive Waste Disposal System", JNC TN8400 99-070 (1999).
3. T. Shibutani, T. Suyama, and M. Shibata: "Distribution Coefficient of Radionuclides on Rocks for Performance Assessment", JNC TN8410 99-050 (1999), in Japanese.
4. H. Sato: "Diffusivity Database (DDB) for Major Rocks: Database for the Second Progress Report", JNC TN8400 99-065 (1999).
5. Japan Nuclear Cycle Development Institute: "The Draft Second Progress Report on Research and Development for the Geological Disposal of HLW in Japan –H12 Project to Establish Technical Basis for HLW Disposal in Japan: Supporting Report 3–", JNC TN1400 99-013 (1999).
6. S. Tajima: Denki-kagaku-tsuron (An Introduction of Electrochemistry), Kyoritsu Press, Tokyo (1986), in Japanese.
7. P. M. Mathew, P. A. Kuegger, and M. Krause: "Diffusion of Lead from a Perforated Titanium –Shell Lead-Matrix Lead Container–", in Scientific Basis for Nuclear Waste Management XV, edited by C. G. Sombret (Mater. Res. Soc. Proc. **257**, Pittsburgh, PA, 1992), pp.431-438.
8. F. E. Goodwin, P. M. Mathew, and R. J. Serme: "North American Studies on Lead Mobility in Simmulated Nuclear Waste Repository Environments", Proc. Int. Conf. on Radioactive Waste Management and Environmental Restoration, Vol. **19**, pp.303-320 (1995).
9. H. Sato, T. Ashida, Y. Kohara, and M. Yui: "Study on Retardation Mechanism of ^{3}H, ^{99}Tc, ^{137}Cs, ^{237}Np and ^{241}Am in Compacted Sodium Bentonite", in Scientific Basis for Nuclear Waste Management XVI, edited by C. G. Interrante and R. T. Pabalan (Mater. Res. Soc. Proc. **294**, Pittsburgh, PA, 1993), pp. 403-408.
10. T. Eriksen, A. Jacobsson, and R. Pusch: "Ion Diffusion through Highly Compacted Bentonite", SKBF/KBS TR 81-06 (1981).
11. H. Sato, T. Ashida, Y. Kohara, M. Yui, and N. Sasaki: "Effect of Dry Density on Diffusion of Some Radionuclides in Compacted Sodium Bentonite, Journal of Nuclear Science and Technology, Vol. **29**, No.9, pp.873-882 (1992).
12. H. Sato: "Measurements of Apparent Diffusion Coefficients (Da) for Cs(I), Ni(II), and Se(IV) in Bentonite with Silica Sand", JNC TN8400 99-060 (1999).
13. J. Crank: The Mathematics of Diffusion, 2nd ed., Pergamon Press, Oxford (1975).
14. Y.Fujikawa: Densanki-niyoru-henbibunhouteishiki-no-kaihou (Analytical Method for Partial Differential Equation by Computer), Science Library, Tokyo (1971), in Japanese.
15. H. Sato and T. Shibutani: "Study on Adsorption and Diffusion Mechanism of Nuclides in Buffer Material and Geosphere", PNC Technical Review No.91, PNC TN8410 94-284, pp.71-89 (1994), in Japanese.
16. H. Sato and M. Yui: "Diffusion Behavior for Se and Zr in Sodium Bentonite", in Scientific Basis for Nuclear Waste Management XVIII, edited by T. Murakami and R. T. Ewing (Mater. Res. Soc. Proc. **353**, Pittsburgh, PA, 1995), pp.269-276.
17. Y. Tachi, Y. Kohara, N. Uchidate, and T. Shibutani: "Diffusion Behavior of Pu and Am in Compacted Bentonite", JNC TN8400 99-089 (1999), in Japanese.
18. H. Sato: "Diffusion Behaviour of Se(-II) and Sm(III) in Compacted Sodium Bentonite", Radiochimica Acta **82**, pp.173-178 (1998).
19. H. Sato and M. Yui: "Diffusion of Ni in Compacted Sodium Bentonite", Journal of Nuclear Science and Technology Vol.**34**, No.3, pp.334-336 (1997).
20. K. Idemitsu, H. Furuya, and Y. Inagaki: "Diffusion of Corrosion Products of Iron in

Compacted Bentonite", in Scientific Basis for Nuclear Waste Management XVI, edited by C. G. Interrante and R. T. Pabalan (Mater. Res. Soc. Proc. **294**, Pittsburgh, PA, 1993), pp.467-474.

21. K. Idemitsu, H. Furuya, Y. Tachi, and Y. Inagaki: "Diffusion of Uranium in Compacted Bentonite in the Presence of Carbon Steel", in Scientific Basis for Nuclear Waste Management XVII, edited by A. Barkatt and R. A. Van Konynenburg (Mater. Res. Soc. Proc. **333**, Pittsburgh, PA, 1994), pp.939-946.
22. K. Idemitsu: "Diffusion of Uranium in the Bentonite in the Presence of Carbon Steel", Radioactive Waste Research, Vol.1, No.1, pp.43-52 (1994), in Japanese.
23. B. Baeyens and M. H. Bradbury: "A Quantitative Mechanistic Description of Ni, Zn and Ca Sorption on Na-Montmorillonite –Part II: Sorption Measurements", PSI Bericht Nr. 95-11 (1995).
24. M. Ito, M. Okamoto, M. Shibata, Y. Sasaki, T. Danbara, K. Suzuki, and T. Watanabe: "Bentonaito-no-koubutsu-sosei-bunseki (Mineral Composition Analysis of Bentonite)", PNC TN8430 93-003 (1993), in Japanese.
25. M. Ito, M. Okamoto, K. Suzuki, M. Shibata, and Y. Sasaki: "Bentonaito-no-koubutsu-sosei-bunseki (Mineral Composition Analysis of Bentonite)", Journal of the Atomic Energy Society of Japan, Vol.**36**, No.11, pp.1055-1058 (1994), in Japanese.
26. Y. Kuroda, K. Idemitsu, H. Furuya, Y. Inagaki, and T. Arima: "Diffusion of Technetium in Compacted Bentonites in the Reducing Condition with Corrosion Products of Iron", in Scientific Basis for Nuclear Waste Management XX, edited by W. J. Gray and I. R. Triay (Mater. Res. Soc. Proc. **465**, Pittsburgh, PA, 1997), pp.909-916.
27. T. E. Eriksen: "Some Notes on Diffusion of Radionuclides through Compacted Clays", SKB Technical Report 89-24, Royal Institute of Technology (1989).
28. T. E. Eriksen and M. Jansson: "Diffusion of I^-, Cs^+ and Sr^{2+} in Compacted Bentonite –Anion Exclusion and Surface Diffusion", SKB Technical Report 96-16, Royal Institute of Technology (1996).
29. D. W. Oscarson: "Surface Diffusion: Is It an Important Transport Mechanism in Compacted Clays?", Clays and Clay Minerals Vol.**42**, No.5, pp.534-543 (1994).
30. J. O. Lee, K. J. Lee, and Won J. Cho: "Sorption and Diffusion of I-125 and Sr-90 in a Mixure of Bentonite and Crushed Granite Buckfill of a Radioactive Waste Repository", Radiochimica Acta **76**, pp.143-151 (1997).
31. T. Keii and Y. Ono: "Kasseika-enerugii (Activation Energy)", Kyoritsu Press, Tokyo (1985), in Japanese.
32. M. Takano, Y. Torikai, S. Sato, and H. Ohashi: "Diffusion of Tritium in Compacted Sodium Bentonite", 1994 Fall Meeting of the Atomic Energy Society of Japan, K5, p.77 (1994), in Japanese.
33. J. Liu, H. Yamada, T. Kozaki, S. Sato, and H. Ohashi: "Effect of Silica Sand on Diffusion of Sodium Ions in Montmorillonite/Sand Mixture", 2001 Annual Meeting of the Atomic Energy Society of Japan, L31, p.629 (2001).
34. Y. H. Li and S. Gregory: "Diffusion of Ions in Sea Water and in Deep-Sea Sediments", Geochimica et Cosmochimica Acta, Vol.**38**, pp.703-714 (1974).
35. H. Sato: "The Effect of Pore Structural Factors on Diffusion in Compacted Sodium Bentonite", in Scientific Basis for Nuclear Waste Management XXIV (in press).
36. H. Sato: "A Study on Pore Structure of Compacted Bentonite (Kunigel-V1)", JNC TN8400 99-064 (1999).
37. H. Suzuki, M. Shibata, J. Yamagata, I. Hirose, and K. Terakado: "Kansyozai-no-tokuseishiken (I) (Property Measurements for Buffer Materials)", PNC TN8410 92-057 (1992), in Japanese.
38. T. Ashida, T. Shibutani, H. Sato, Y. Tachi, A. Kitamura, and K. Kawamura: "Nuclide Migration Study in the QUALITY –Data Acquisitions for the Second Progress Report–", JNC TN8400 99-083, pp.32-40 (1999), in Japanese.
39. "Kagaku-binran, Kisohen II (Handbook of Chemistry, 2nd Edition)", Nihon-kagakukai (Chemical Society of Japan), p.604 (1974), in Japanese.
40. H. Kato and T. Yato: "Estimation of the Effective Diffusivuty in Sand/Bentonite Mixture", 1997 Fall Meeting of the Atomic Energy Society of Japan, I39, p.681 (1997), in Japanese.

APPENDIX 1

The Derivation of Generalized Equation Used in order to Calcalate Smectite Partial Density

Figure App.1-1 shows components of bentonite added silica sand with an arbitrary content. The bentonite with silica sand is composed of pore, smectite, impurity and silica sand added with an arbitrary content. The dry density of bentonite ρ_d in this case is calculated by the following equations.

$$\rho_d = \frac{W_m + W_{im} + W_s}{V_T} = \frac{W_m + W_{im} + W_s}{V_p + V_m + V_{im} + V_s} \qquad \text{(App.1-1)}$$

Where Wm is the weight of smectite contained, Wim is the weight of impurities contained, Ws is the weight of silica sand added, VT is the total volume of bentonite containing pore, Vp is the pore volume, Vm is the smectite solid volume, Vim is the volume of impurities, and Vs is the silica sand volume.

The smectite content in bentonite fm is expressed as follows.

$$f_m = \frac{W_m}{W_m + W_{im}} \qquad \text{(App.1-2)}$$

The silica sand content in bentonite is calculated as follows.

$$f_s = \frac{W_s}{W_m + W_{im} + W_s} \qquad \text{(App.1-3)}$$

The smectite partial density ρ_{dm} is calculated from the next equation.

$$\rho_{dm} = \frac{W_m}{V_p + V_m} = \frac{W_m}{V_T - V_{im} - V_s} \qquad \text{(App.1-4)}$$

The average pure density of impurities ρ_{im} is calculated as follows.

$$\rho_{im} = \frac{W_{im}}{V_{im}} \qquad \text{(App.1-5)}$$

The pure density of silica sand ρ_s is calculated as follows.

$$\rho_s = \frac{W_s}{V_s} \qquad \text{(App.1-6)}$$

Substituting equations (App.1-1), (App.1-5) and (App.1-6) into equation (App.1-4), the following relation can be obtained.

$$\rho_{dm} = \frac{W_m}{\dfrac{W_m + W_{im} + W_s}{\rho_d} - \dfrac{W_{im}}{\rho_{im}} - \dfrac{W_s}{\rho_s}} \qquad \text{(App.1-7)}$$

Equation (App.1-2) can be rearranged as follows.

$$f_m(W_m + W_{im}) = W_m$$

$$\because\ W_{im} = \left(\frac{1-f_m}{f_m}\right)W_m \qquad \text{(App.1-8)}$$

Equation (App.1-3) can be rearranged as follows.

$$W_s = f_s(W_m + W_{im} + W_s)$$

$$\because\ W_s = \left\{\frac{f_s}{(1-f_s)f_m}\right\}W_m \qquad \text{(App.1-9)}$$

Substituting equations (App.1-8) and (App.1-9) into equation (App.1-7), we have the following equations.

$$\begin{aligned}
\rho_{dm} &= \frac{W_m}{\dfrac{W_s}{f_s \cdot \rho_d} - \left(\dfrac{1-f_m}{\rho_{im} \cdot f_m}\right)W_m - \dfrac{W_s}{\rho_s}} \\
&= \frac{W_m}{\dfrac{f_s \cdot W_m}{(1-f_s)f_m \cdot \rho_d \cdot f_s} - \left(\dfrac{1-f_m}{\rho_{im} \cdot f_m}\right)W_m - \dfrac{f_s \cdot W_m}{(1-f_s)f_m \cdot \rho_s}} \\
&= \frac{1}{\dfrac{\rho_s \cdot \rho_{im} - (1-f_m)(1-f_s)\rho_d \cdot \rho_s - f_s \cdot \rho_d \cdot \rho_{im}}{(1-f_s)f_m \cdot \rho_d \cdot \rho_s \cdot \rho_{im}}} \\
&= \frac{(1-f_s)f_m \cdot \rho_d}{1 - \dfrac{(1-f_m)(1-f_s)}{\rho_{im}}\rho_d - \dfrac{f_s}{\rho_s}\rho_d} \\
&= \frac{(1-f_s)f_m \cdot \rho_d}{1 - \left\{\dfrac{(1-f_m)(1-f_s)}{\rho_{im}} + \dfrac{f_s}{\rho_s}\right\}\rho_d} \qquad \text{(App.1-10)}
\end{aligned}$$

Thus, the following relation (equation (5.3-2)) can be finally derived.

$$\rho_{dm} = \frac{(1-f_s)f_m \cdot \rho_d}{1 - \left\{\dfrac{(1-f_m)(1-f_s)}{\rho_{im}} + \dfrac{f_s}{\rho_s}\right\}\rho_d}$$

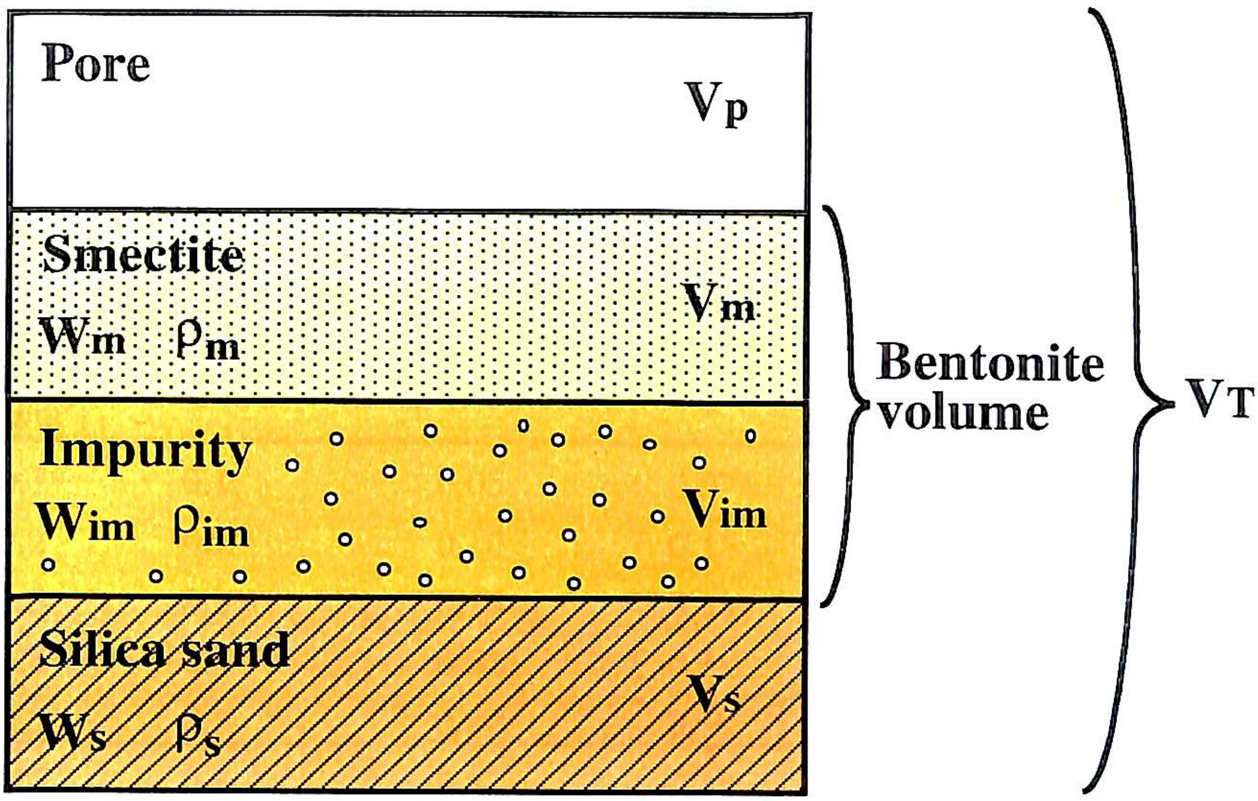

Figure App.1-1 Components of bentonite added silica sand with an arbitrary content

APPENDIX 2

Calculated Results of Smectite Partial Density as a Function of Dry Density of Various Kinds of Bentonites

Table App.2-1 shows the calculated results for smectite partial density as a function of dry density of bentonite with respect to various kinds of bentonites.

Table App.2-1 Calculated results for smectite partial density (ρ_{dm}) with respect to various kinds of bentonites

Dry density [Mg/m^3]	ρ_{dm} for Kunipia-F	ρ_{dm} for Kunigel-V1	ρ_{dm} for MX-80	ρ_{dm} for Avonlea bentonite	ρ_{dm} for Korean bentonite
0.1	0.1	0.05	0.076	0.081	0.087
0.2	0.2	0.10	0.15	0.16	0.18
0.3	0.3	0.16	0.23	0.25	0.26
0.4	0.4	0.22	0.31	0.33	0.35
0.5	0.5	0.28	0.39	0.42	0.45
0.6	0.6	0.33	0.48	0.50	0.54
0.7	0.7	0.40	0.56	0.59	0.63
0.8	0.8	0.47	0.65	0.68	0.72
0.9	0.9	0.54	0.74	0.77	0.82
1.0	1.0	0.61	0.83	0.86	0.91
1.1	1.1	0.69	0.92	0.96	1.01
1.2	1.2	0.77	1.0	1.05	1.11
1.3	1.3	0.86	1.11	1.15	1.21
1.4	1.4	0.95	1.21	1.25	1.31
1.5	1.5	1.0	1.31	1.35	1.41
1.6	1.6	1.14	1.41	1.45	1.51
1.7	1.7	1.24	1.51	1.56	1.61
1.8	1.8	1.35	1.62	1.66	1.71
1.9	1.9	1.47	1.73	1.77	1.82
2.0	2.0	1.59	1.84	1.88	1.93